CHARACTERIZATION OF THE ADSORPTION BEHAVIOUR OF AQUEOUS Cd(II) AND Ni(II) IONS ON NANOPARTICLES OF ZERO-VALENT IRON

A Thesis Submited to
the Graduate School of Engineering and Science of
İzmir Institute of Technology
in Partial Fulfillment of the Requirements for the Degree of

MASTER OF SCIENCE

in Chemistry

by
Nazlı EFECAN

July 2008
İZMİR

We approve the thesis of **Nazlı EFECAN**

_____

Assoc. Prof. Dr. Talal SHAHWAN
Supervisor

_____

Prof. Dr. Çetin GÜLER
Committee Member

_____

Prof. Dr. Serdar ÖZÇELİK
Committee Member

17 July 2008
Date

_____

Prof. Dr. Levent ARTOK
Head of the Chemistry Department

_____

Prof. Dr. Hasan BÖKE
Dean of the Graduate School of
Engineering and Sciences

ACKNOWLEDGEMENTS

I would like to thank my supervisor Assoc. Prof. Dr. Talal SHAHWAN, for his supervision, guidance, endless support, and encouragement throughout my thesis study.

Special thanks to group members of Materials Research Center, Evrim YAKUT, Duygu OĞUZ, and Gökhan ERDOĞAN for their helps in XRD, SEM and BET analyses. I would like to thank reasearch specialist Dr. Sinan YILMAZ for his helps in AAS analysis. For TEM and EELS analyses, I owe my thanks to Dr. Ingo Lieberwirth at Max Planck Institue for Polymer Research, Mainz.

Also, I would like to thank my friends Özge TUNUSOĞLU, Çağrı ÜZÜM, Meral KARACA, Ezel BOYACI, Semira ÜNAL, Ayşegül ŞEKER for their helps during laboratory studies.

Finally, I would like to thank my family for their motivation, support and endless encouragement.

ABSTRACT

CHARACTERIZATION OF THE ADSORPTION BEHAVIOUR OF AQUEOUS Cd(II) AND Ni(II) IONS ON NANOPARTICLES OF ZERO-VALENT IRON

Iron nanotechnology is recently concieved as a promising tool in environmental remediation. By virtue of their high surface/volume ratio, iron nanoparticles were shown to demonstrate outstanding sequestration capacity for various organic and inorganic pollutants.

In this work iron nanoparticles were synthesized using the borohydride-reduction method. The obtained material showed chain like morphology, with the diameter of the nanoparticles being with in 20-80 nm range. HR-TEM images showed that the nanoparticles have a core-shell structure, with the core containing iron in its zero-valent state, while the shell is composed of iron oxides (Fe_2O_3, Fe_3O_4, FeOOH)and is generally < 3 nm in thickness.

Nano-sized zero valent iron (nZVI) was then tested as a sorbent material for aqueous Cd^{2+} and Ni^{2+} ions. The uptake of these ions was investigated under various experimental conditions like time, concentration, pH, repititive application, and liquid/solid ratios. In addition, the uptake of these ions was compared with that of Cu^{2+}, Zn^{2+}, and Sr^{2+} in order to assess the effect of the reduction potential on the extent of removal.

The results showed that nZVI is a very effective sorbent in terms of both kinetics and capacity of removal of the ions. Under the investigated conditions, the uptake reached equilibrium in less than one hour of contact time. Up to the initial concentration of 500 mg/L, the ions were removed almost completely utilizing an nZVI amount of 0.025 g and a solution volume of 10 ml. According to XRD and XPS results, both of Cd^{2+} and Ni^{2+} ions were fixed by nZVI through a non-reductive mechanism, that seems to be dominated by interaction of these ions with the exposed iron oxyhydroxide groups at the interface with the solution.

ÖZET

Cd(II) VE Ni(II) İYONLARININ SIFIR-DEĞERLİKLİ DEMİR PARÇACIKLARI TARAFINDAN ADSORBLANMA DAVRANIŞLARININ KARAKTERİZASYONU

Demir nanoteknolojisi son zamanlarda çevre iyileştirilmesinde geliştirilen ümit verici araçlardan biridir. Büyük yüzey / hacim oranının sağladığı yararla, organik ve anorganik kirleticilerin tutulmasında demir nanoparçacıkların üstün bir kapasiteye sahip olduğu son zamanlarda kanıtlanmaktadır.

Bu çalışmada, demir nanoparçacıklar borhidrür-indirgeme metodu kullanılarak sentezlenmiştir. Sentezlenen malzemenin, 20-80 nm civarında büyüklüğe ve zincir benzeri yüzey yapısına sahip olduğu gösterilmiştir. Malzemenin HR-TEM fotoğrafları nanoparçacıklarının çekirdek-kabuk şekline sahip olduğunu, kabuğun demir oksitlerden (Fe_2O_3, Fe_3O_4, FeOOH) meydana gelirken, çekirdeğin sıfır yüklü demir içerdiğini göstermiştir.

Nano boyutlu sıfır yüklü demir daha sonra sudaki Cd^{2+} ve Ni^{2+} iyonlarının adsorblanmasında kullanılmıştır. Bu iyonların tutunması, zaman, konsantrasyon, pH, tekrarlanabilirlik ve sıvı/katı oranı gibi farklı deneysel koşullar altında araştırılmıştır. Buna ek olarak, indirgenme potansiyelinin tutunmadaki etkisini değerlendirmek için Cu^{2+}, Zn^{2+}, ve Sr^{2+} iyonlarının tutunması Cd^{2+} ve Ni^{2+} tutunmalarıyla karşılaştırılmıştır.

Sonuçlara göre, sıfır yüklü demir nano parçacıklar hem kinetik açıdan hem de adsorpsiyon kapasitesi açısından iyonların uzaklaştırılmasında oldukça etkili olmaktadır. Deneysel koşullar altında, iyonların tutunmaları bir saatten az bir süre içerisinde dengeye ulaşmaktadır. 0.025 g sıfır değerlikli demir nano parçacıkları (10 mL çözeltide) gibi küçük bir miktarı kullanarak, 500 mg/L konsantrasyonuna kadar, Cd^{2+} ve Ni^{2+} iyonlarının neredeyse tamamen uzaklaştırılmıştır.XRD veXPS sonuçlarına göre, hem Ni^{2+} hem de Cd^{2+} iyonları sıfır yüklü demir nanoparçacıklar tarafından indirgeyici olmayan, ve daha çok nanoparçacıkların yüzüyinde bulunan demir oksohidroksit grupları içeren bir mekanizmayla tutunmuştur.

To my family.....

TABLE OF CONTENTS

LIST OF FIGURES

Figure **Page**

LIST OF TABLES

Table **Page**

CHAPTER 1

INTRODUCTION

1.1. Pollution in Natural and Waste Waters

Water pollution is among the most challenging environmental problems in modern world. Pollutants are increasingly affecting natural and wastewaters in the forms of heavy metals, organic chemicals (e.g. chlorinated organics such as trichloroethane, carbon tetrachloride etc.), inorganic anions (e.g. nitrate, pherchlorate etc.), and bacteria.

Heavy metals are a group of elements that include antimony, arsenic, bismuth, cadmium, cerium, chromium, cobalt, copper, gallium, gold, iron, lead, manganese, mercury, nickel, platinum, silver (Alloway 2005). These elements possess densities above 4 g/cm^3, and their specific gravity is greater than 5. Small amounts of these elements are common in our environment and diet and are actually necessary for good health, but large amounts of any of them may cause acute or chronic toxicity (poisoning). Heavy metals may enter the human body through food, water, air, or absorption through the skin when they come in contact with humans in agriculture and in manufacturing. But the most important enterence occur with water, because of this effective remediation of polluted water is essential for humans health. This work is about the stabilization of the different heavy metals in aqueous media; cadmium, copper, nickel, strontium and zinc.

Nickel is a metal found in natural deposits as ores containing other elements. The greatest use of nickel is in making stainless steel and other alloys. It is also used for plating and as a green tint in glass. Nickel plays numerous roles in the biology of microorganisms and plants, though they were not recognized until the 1970s. In fact urease (an enzyme which assists in the hydrolysis of urea) contains nickel. The NiFe-hydrogenases contain nickel in addition to iron-sulfur clusters. Nickel is an important cause of contact allergy, partly due to its use in jewelary intended for pierced ears. Nickel allergies affecting pierced ears are often marked by itchy, red skin (Wikipedia 2008a). An uptake of too large quantities of nickel has the other following

consequences; Birth defects, asthma and chronic bronchitis. Recommended daily intake of nickel is <1 mg.

Cadmium is used largely in batteries and pigments, for example in plastic products. Cadmium is an occupational hazard associated with industrial processes such as metal plating and the production of nickel-cadmium batteries, pigments, plastics, and other synthetics (Cook and Morrow 1995). Cadmium poisining in humans causes serious consequences. Among them are high blood preasure, kidney damage, destruction of red blood cells. Because the physiological action of cadmiums is very similar to that of zinc, cadmium can replace zinc in some enzymes and impair its catalytical activity (Manahan 1991). The maximum contaminant level (MCL) for cadmium in drinking water is 0.01 mg/L (10 ug/L) according to Environmental Protection Agency (EPA).

Copper is used as an electrical conductor, heat conductor, in the water pipes, pigments, and chemical equipment. Copper is an important element for all plants and animals. It is usually found in bloodstream, as a co-factor various elements, and copper-based pigments. But in sufficient amount it can be poisonous and cause cancer (Wikipedia 2008b). Sources of copper contamination in natural aqueous media may be mining, domestic and industrial wastewaters (Manahan 1991, Evangelou 1998). Copper is a component of several enzymes necessary for normal metabolic functions. The Recommended Daily Allowance (RDA) of copper for adults is 0.9 milligrams (mg). An inherited condition called Wilson's disease causes the body to retain copper, since it is not excreted by the liver into the bile. This disease, if untreated, can lead to brain and liver damage (Wikipedia 2008c).

As a pure metal strontium is being used in strontium 90%-aluminium 10% alloys of an eutectic composition for the modification of aluminium-silicon casting alloys. The primary use for strontium compounds is in glass for colour television cathode ray tubes to prevent X-ray emission. The human body absorbs strontium as if it were calcium. The stable forms of strontium does not effect the human body directly but the radioactive ^{90}Sr can cause bond disorders and diseases, including bond cancer (Wikipedia 2008d). Because strontium is a non-essential, trace mineral in human beings, there is no RDA for it.

Zinc is the fourth most common metal in use, trailing only iron, aluminium, and copper in annual production. It is used to galvanize steel to prevent corrosion, in die casting notably in the automobile industry. Zinc is an essential element, necessary for

sustaining all life. It is estimated that 3,000 of the hundreds of thousands of proteins in the human body contain zinc prosthetic groups, one type of which is the so-called zinc finger. Zinc is an activator of certain enzymes, such as carbonic anhydrase. Carbonic anhydrase is important in the transport of carbon dioxide in vertebrate blood. It is also required in plants for leaf formation, the synthesis of indole acetic acid (auxin) and anaerobic respiration (alcoholic fermentation). Zinc is found in oysters, and to a far lesser degree in most animal proteins, beans, nuts, almonds, whole grains, pumpkin seeds and sunflower seeds (Wikipedia 2008e). The RDA value for zinc is 10 mg per day, the excess amount of zinc reduced levels of lipoproteins and immune function.

Some of the chemical and physical properties of the cations applied in this study are given in Table 1.1.

Table 1.1. The chemical properties of elements
(Source: Wikipedia and Web of Elements 2008)

Element	Electronegativity (Pauling Scale)	Oxidation State	Atomic Radius (pm)	Standart Reduction Potential(E^0/V)
Cd	1.69	+2	161	-0.4025
Cu	1.90	+2, +3	149	+0.340
Ni	1.91	+2	135	-0.257
Sr	0.95	+2	219	-2.89
Zn	1.65	+2	142	-0.7926

Groundwater is the water that has collected underground in the spaces between dirt particles and crack within rocks. Groundwater flows underground and may empty into rivers or lakes. Many people rely on groundwater as the source of their daily water needs but its percentage is smaller than the other water sources. It is known that groundwater soruces are under the threat of pollution. Until 1980s cleanup began and the expected reduction produced in contamination levels in groundwater (Thiruvenkatachari, et al. 2007). Groundwater cleaning processes is very expensive and much harder than the surface water (Baird 2001).

Remediation technologies for the contaminated surface and groundwater are given below.

1.2. Water Remediation Methods

There are two general methods for cleaning contaminated water sources: *Ex situ* and *in situ* methods.

Pump-and-treat method, shown in Figure 1.1, is an example to *ex situ* method. Pumps are used to bring polluted groundwater to the surface where it can be cleaned up (*treated*) more easily. To transfer polluted water from its underground reservoir, an *extraction system* is built. This system usually consists of one or more wells equipped with pumps. At the surface, the water goes into a holding tank and then on to a treatment system, where it is cleaned. There are a number of treatment methods which can be used either to destroy the polluting chemicals or to remove them for proper disposal (Environmental Protection Agency Guide 2001).

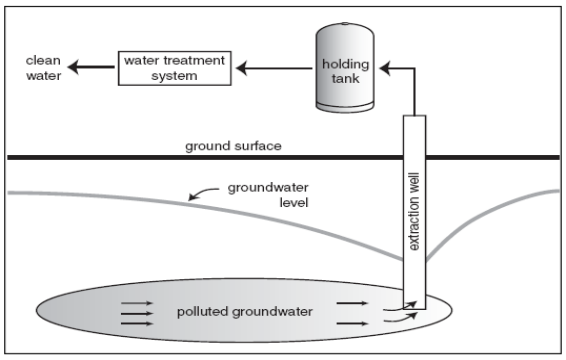

Figure 1.1 Pump and Treat System
(Source : EPA Guide 2001)

Alternatively, *in situ* methods include; direct injection of reactive materials to aquifers, reactive treatment zones and permeable reactive barriers (PRBs). PRBs is the most important technique for this type of methods. As shown in the illustrative diagram in Figure 1.2, PRB is a simple system in which the permenant, semi permenant or replaceable reactive media of PRBs is placed on the path of the polluted groundwater which passes through the PRBs reactive media. The reactive media decreases toxicity of the contaminants in water or transform them into immobile species. The reactive media

are classified based on the target pollutant and the mechanism of removal as given in Table 1.2. (Thiruvenkatachari et al. 2007).

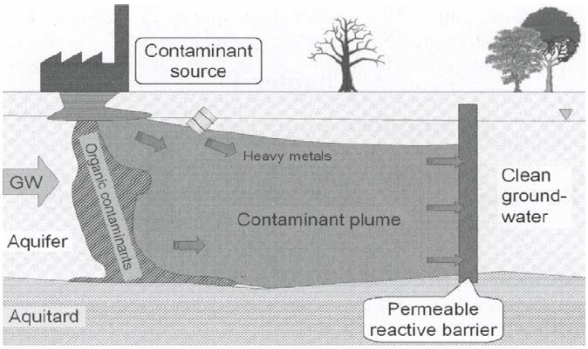

Figure 1.2 Scheme of PRBs (GW, groundwater flow direction)
(Source: Roehl, et al. 2005)

Table 1.2 Target mechanism of removal and reactive materials
(Source: Thiruvenkatachari, et al.2007)

Target and mechanism of removal	**Reactive materials**
Inorganics-sorption or substitution barriers	Activated carbon, activated alumina, oxyhydroxides, magnetite,
Inorganics-precipitation barriers	Biota, dithionite, ferrous hydroxides, hydrogen sulfide gas, zero-valent metals
Inorganics-degradation barriers	Biota, zero-valent metals
Organics-degradation barriers	Ferrous minerals, oxygen release, ultramicrobacteria, zero-valent metals
Organics-sorption barriers	Zeolite, activated carbon, clays

Zero-valent materials are important for the PRBs facilities. Zero-valent iron (ZVI) is the most common one for the reactive zero-valent materials. Over the past decade, PRB's have been developed and used to treat groundwater contaminated by different pollutants (Blowes, et al. 2000). In these barriers, zero-valent iron (ZVI) can be used as a reactive material due to its great ability to reduce and stabilise different

types of ions. When zero-valent iron is synthesised on the nanoscale, the uptake capacity increased largely due to the increase in surface area and density of reactive sites (Nurmi, et al.2005). The application of nZVI particles for *in situ* environmental remediation have been tried by direct injection (Figure 1.3). This technology is considered to offer several advantages: (1) effective for transformation of a large variety of environmental contaminants, (2) inexpensive and (3) non-toxic (Wei-xian Zhang 2003). On the other hand, the technology is reported to suffer from some uncertainties. Among these is the cost associated with the required amount of nZVI. (Tratnyek and Jhonson 2006). Another major restriction is related with appropriate storage of iron nanoparticles prior to usage for a long time without significant oxidizing (Li, et al.2006)

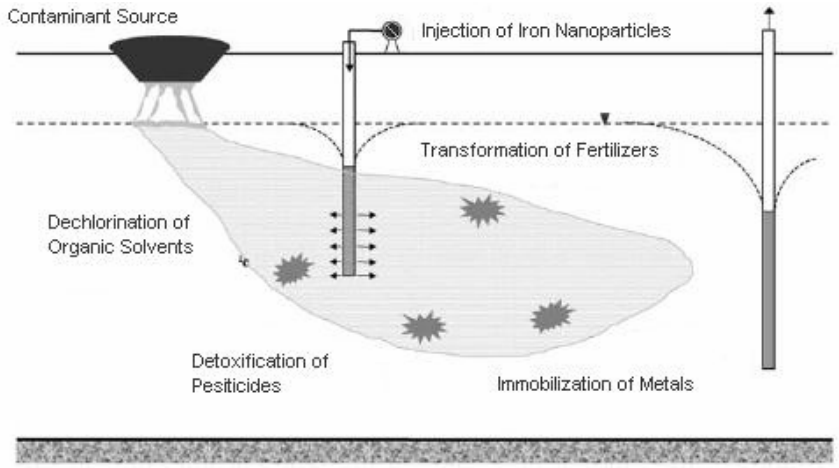

Figure 1.3 Nanoscale ZVI particles for *in situ* remediation
(Source: Wei-xian Zhang 2003)

1.3 Nanoscaled Zero-Valent Iron (nZVI)

Iron is a transition metal with atomic number 26. It is placed in group 8 and period 4 of periodic table. It possess several isotopes but the most important ones are: radioactive ^{54}Fe with half-life >$3.1x10^{22}$ years (5.8%), stable ^{56}Fe (91.72%), stable ^{57}Fe (2.2%), and stable ^{58}Fe (0.28%). The oxidation states and reduction potentials of iron specei are shown in Figure 1.4.

Iron is the sixth-most abundant element in the world. It is a very reactive element and is oxidized very rapidly and as a result it usually exist in nature in the form of magnetite (Fe_3O_4) and hematite (Fe_2O_3). Iron is an essential element for living organisms through fascilitating oxygen transport on the hemoglobin and myoglobin proteins as it can bind oxygen easily via redox reaction. Low iron limits in blood can cause anemia. Excess amount of iron can, however, be toxic because free ferrous iron reacts with peroxides to produce free radicals that can damage DNA. Iron Tolerable Upper Intake Level (UL) for adults is 45 mg/day, for children under fourteen, UL is 40 mg/day. (Wikipedia 2008f.)

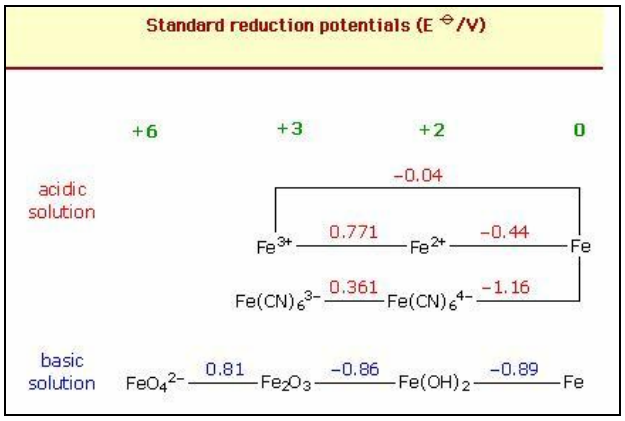

Figure 1.4 Standart reduction potentials of iron species
(Source: Web of Element 2008)

There are reports that zero-valent iron has greater activity toowards contaminants by its highly reducing character. When zero-valent iron is synthesized in

nano scale its surface area and reactivity increases largely. This increase in reactivity can amount to 30 times that of iron powder (Tratnyek and Johnson 2006). The surface area-size relationship is demonstrated in Figure 1.5.

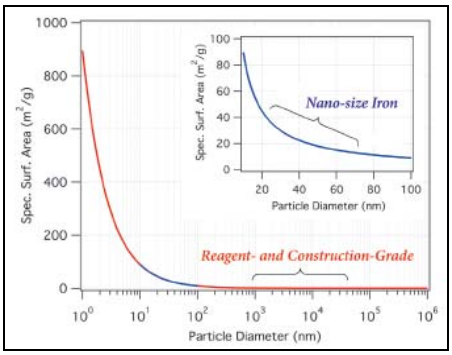

Figure 1.5 Specific Surface Area vs. Particle Diameter
(Source: Tratnyek and Johnson 2006)

Synthesis of nanoscale zero-valent iron methods can be acheived by a variety of physical and chemical synthesis techniques. A summary of these techniques was recently outlined in a review paper on the topic by Li and coworkers (Li, et al.2006). Liquid phase reduction method is among the most common method. In this method Fe^{2+} and Fe^{3+} ions are reduced to zero-valent iron with sodium borohydride, a strong reducing agent. Because of this, liquid phase reduction method is also called borohydride reduction. This method is very simple because it needs only two common reactants without a need to any special equipment (Zang and Elliot 2006). The reduction process is thought to occur through the reaction:

$$Fe^{2+} + 2BH_4^- + 6H_2O \rightarrow Fe^0 + 2B(OH)_3 + 7H_2 \uparrow \qquad (1.1)$$

The synthesized nZVI particles are usually in spherical shape and have a core-shell structure. The nZVI particles are unstable in atmospheric conditions and it tends to form oxides/hydroxides in the forms Fe_2O_3, Fe_3O_4 and FeOOH. The shell consist of oxides and hydroxides and the core consist of Fe^0. (Martin et al. 2008). This structure is conceptualized in the model given in Figure 1.6. The oxide shell has a thickness of

about 5 nm and consists of iron oxide (Li and Zhang 2007). Alternatively, Wang, et al. stated that the surface of nZVI is mainly an iron-boron noncrystalline alloy and that the slow oxidation of the nanoparticles can be ascribed to this (Wang et al. 2006). The core of the nanoparticle forms the source of electrons in the redox reaction. The shell plays also important role in the fixation of ions by the external surface of the nanoparticles. The overall process can be thought to consist of three mechanism (Zhang et al. 2006). These mechanisms are : (i) physical sorption that takes place for cations having standart reduction potential , E^0, that is more negative than or close to that of Fe, (ii) both sorption and chemical reduction arises for cations having E^0 sligthly more positive than that of Fe and (iii) only chemical reduction occurs for cations with E^0 higher than that of Fe.

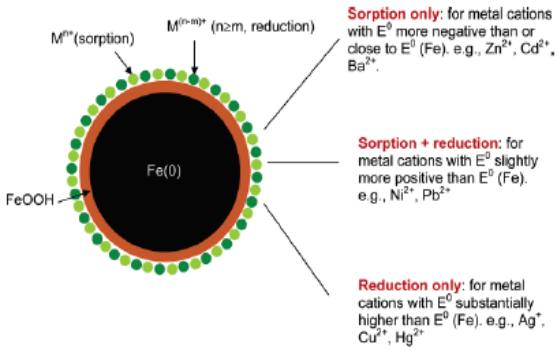

Figure 1.6 A model for core-shell structure of nZVI and uptake mechansims of metals (Source: Li and Zang 2007)

So far, nZVI has been tested under laboratory conditions for the destruction, stabilization, and/or removal of a variety of chemicals. These include various organic compounds and inorganic cations/anions. Among the organic compounds are chlorinated hydrocarbons (Li, et al. 2006), polychlorinated biphenyls , chlorinated ethenes , heavy metals such as Pb^{2+}, Cr^{6+}, Ni^{2+}, As^{3+}, As^{5+}, Cd^{2+}, Cu^{2+}, Zn^{2+}, Co^{2+} and Ba^{2+} (Li, et al. 2006), and inorganic anions, nitrate, sulphate, phosphate (Thiruvenkatachari 2007).

1.4 Aim of the Study

This study focuses on the synthesis of zero-valent iron nanoparticles, characterization of the material, and its application for the removal Ni^{2+} and Cd^{2+} ions under different experimental conditions. Literature resources include a brief investigation of the interaction of the two ions with iron nanoparticles in terms of the fixation mechanism (Li and Zhang 2006), (Lindsay, et al. 2008). This study provides comprehensive investigation that includes the effects of contact time, initial metal concentration, pH of solution, repetitive loading, dose (mass of sorbent), and competing ions. Different characterization techniques were employed in this study. These include X-Ray Powder Diffraction (Powder XRD), Scanning Electron Microscopy (SEM), Transmission Electron Microscopy (HR-TEM), X-Ray Photoelectron Spectroscopy (XPS), Energy Dispersive X-Ray Spectroscopy (EDS), and Electron Energy Loss Spectroscopy (EELS). Atomic Absorption Spectroscopy (AAS) analysis is performed to determine the aqueous concentrations of the cations used in this work.

CHAPTER 2

EXPERIMENTAL

2.1. Chemicals and Reagents

Throughout this study $Fe.Cl_2.4H_2O$ (Sigma-Aldrich 22029-9), $NaBH_4$ (Aldrich 4511-2), absolute ethanol (Riedel-de Haën 32221), $CdCl_2$ (Fluka 20899), $Cu(NO_3)_2.2.5H_2O$ (Riedel-de Haën 31288), $NiCl_2.6H_2O$ (Carlo Erba 464645), $SrCl_2.6H_2O$ (Merck 393065), $ZnN_2O_6.6H_2O$ (Fluka 96482), KCl (Riedel-de Haën 31248), CsCl (Merck 0025), were used without further purification or process. All standarts solutions were prepared in high purity water (Millipore, 18.2 Ω).

2.2. Applied Methods

The characterization of nZVI prior to and following uptake from metal cations in addition to the concentration of these cations in the liquid phase were performed using the techniques described in the following sections.

2.2.1. Powder X-Ray Diffraction (PXRD)

X-ray is a type of electromagnetic radiation with a wavelength in the range of 10^{-5} A^0 to 100 A^0. X-rays are placed between gamma-ray region and the ultraviolet region on the electromagnetic spectrum. X-rays are nearly in atomic scale and for this reason crystalline structures at atomic level can be determined using this radiation type. X-ray powder patterns can be used as finger prints for crystalline solids, because each crystalline solid has its own characteristic X-ray pattern in the literature. Unknown

materials can be determined with this pattern databases. (Skoog, et al. 1998). A schematic diagram showing the components in an XRD instrument is given in Figure 2.1.

Throughout the study, a Philips X'Pert Pro instrument at the Centre of Material Research in İzmir Institute of Technology was used for Powder XRD analysis. The samples were first gorund, then introduced for analysis in the special sample holder. Cu Kα radiation at wavelength of 1.54 A^0 was used as the source.

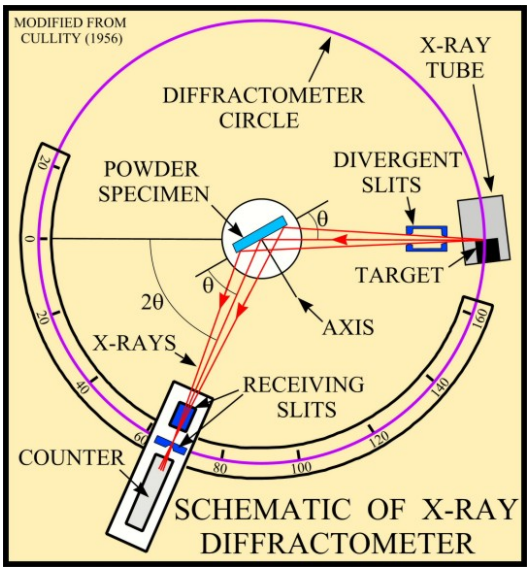

Figure 2.1. Schematic of X-ray Diffractometer
(Source: U. S. Geological Survey 2001)

2.2.2. Scanning Electron Microscopy (SEM)

The scanning electron microscope (SEM) is a type of electron microscope that images the sample surface by scanning it with a high-energy beam of electrons in a raster scan pattern. The electrons interact with the atoms that make up the sample producing signals that contain information about the sample's surface topography, composition and other properties such as electrical conductivity. The energy of the electron beam can range from a few hundred eV to 100 keV. This beam is focused by

one or more condenser lenses into a spot sized 0.4 nm to 0.5 nm. By the help of scanning coils or pairs of deflector plates in the electron optical column beam is deflected horizontally and vertically so that scanning occurs in a raster fashion over a rectangular area of the sample surface. The contact of the source electrons with the sample results in the production of backscattered, secondary and Auger electrons as well as X-ray fluorescence photons and various other photons. Basically, backscattered and secondary electron signals are used to study the surfaces (Skoog, et al. 1998, Strobel and Heineman 1989). Backscattered electrons are elastically reflected source electrons and secondary electrons from the surface atoms. Those are detected by photomultiplier tube and finally, 2D or 3D image is displayed on the CTR monitor. High vacuum media is essential for the quality of analysis. The components of an SEM instrument is shown in the schematic diagram in Figure 2.2.

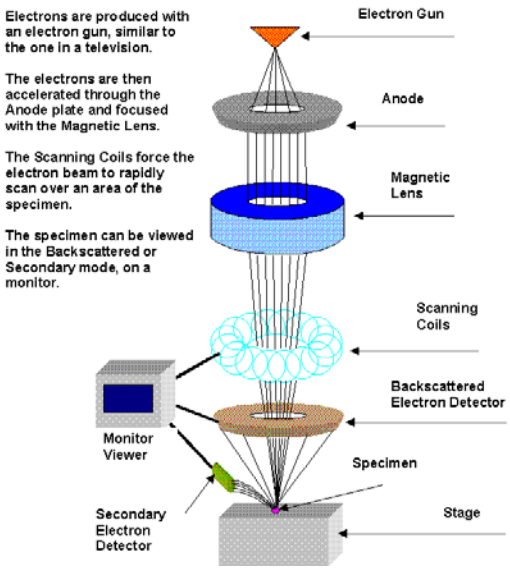

Figure 2.2. Schematic of Scanning Electron Microscopy
(Source: Renssealer Polytechnic Institute 2008)

Another mode of operation performed using the same instrument is the Energy-Dispersive X-ray Analysis (EDX). This type of analysis takes advantage of the x-rays emitted by the atoms on the surface of the specimen and as a result is useful for determining the elemental composition of solid materials.

Throughout the study, SEM/EDX characterizations were performed by a Philips XL-30S FEG model instrument. The powder samples were attached onto adhesive carbon tapes supported on metalic disks. Sample surfaces were then observed at different magnifications and the images were recorded. Elemental EDX analysis was performed at randomly selected areas on the solid surfaces each being approximately 20μm x 20 μm in dimensions. EDX mapping was carried out at 1000x magnification with a voltage applied at 18 kV under vacuum conditions of $3.5x10^{-5}$ mbar.

2.2.3. Transmission Electron Microscopy (TEM)

In transmission electron microscopy (TEM), a beam of electrons is transmitted through a specimen to form an image. At the top of the microscope, electrons are emmited by the "light source" and travel through vacuum in the column of the microscope. Just like the glass lenses focusing the ligth in the light microscopes, electromagnetic lenses are used to focus the electrons into a very thin and dense beam. The electron beam then passes through the sample studied. Density of a material present in the sample causes some of the electrons to be scattered and dissappeared from the beam. Unscattered electrons hit a fluorescent screen, a layer of photographic or a CCD camera which gives rise to a "shadow image" of the sample with its different parts displayed in varied contrast according to their density (Wikipedia 2008g)

A light microscope presents a magnification that is limited by the wavelength of light while a TEM instrument uses electrons as source and the much lower wavelength of electrons makes thousand times better resolution than a ligth microscope possible. Objects in size of a few Angstroms (10^{-10} m) can be observed by TEM technique. New generation high resolution instruments can be used to study materials in near atomic levels. So TEM is a valuable tool in medical, physical, biological, and materials research (Nobel Web AB 2008).

Altough TEM is one of the most advanced surface analysis techniques, it is an expensive and destructive technique. There are some restrictions for materials that are sensitive to electron beam radiation, resulting in a loss of crystallinity and mass. Sample peraparation is another problem and it is a specialist issue. The components of a TEM instrument is shown in the schematic diagram in Figure 2.3.

The TEM instrument used in this study was a Tecnai F20 from FEI, Netherlands located at the Max-Planck Institute for polymer research. The instrument was operated at 200 kV acceleration voltage. Samples were prepared for analysis by dispersing some of the sample powder in ethanol using an ultrasonic bath. Subsequently, a drop of the dispersion was applied to a holey carbon TEM support grid; excess solution was blotted by a filter paper.

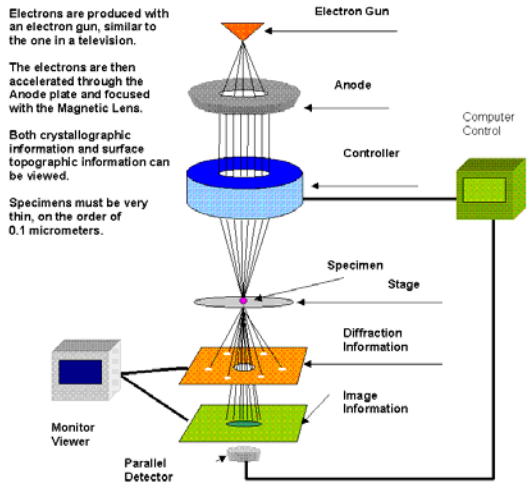

Figure 2.3. Schematic of Transmission Electron Microscopy
(Source : Renssealer Polytechnic Institute)

2.2.4. Electron Energy Loss Spectroscopy (EELS)

When an electron beam is incident into a specimen, part of the electrons is inelastically scattered and undergo partial loss in their energy. Elemental composition and atomic bonding state can be determined by analyzing the energy with the spectroscope attached under the electron microscope. Because the analysed region can be selected from part of the enlarged electron microscopic image, it is possible to analyze very small regions. Moreover, by selecting electrons with a specific loss energy

by a slit so as to image them, element distribution in specimen can be visualized in the form of elemental maps (Kyoto University 2008).

EELS analysis in this study were run at a EM 912 from LEO, Germany operatedat at 120 kV acceleration voltage. The sample preparation is the same as that for TEM.

2.2.5. X-Ray Photoelectron Spectroscopy (XPS)

X-Ray Photoelectron Spectroscopy (XPS) is also known as Electron Spectroscopy for Chemical Analysis (ESCA). This technique is a powerful surface technique for determining the chemical composition, and to provide information about the structure and oxidation state of the elements under interest. The theory is based on the detection of kinetic energies of emitted core electrons by source X-ray photons. The energy of photon is fixed and the kinetic energy of the emitted electron can be detected, so binding energy is simply the difference of these two energies. The binding energy of an emitted photelectron is characteristic of the atom and orbital form which the electron was emitted. Qualitative and quantitative elemental analysis on the speciment surface can thus be achieved in a very sensitive manner. Moreover, since binding energy of core electron varies slightly with the charge density or chemical environment of the atom under interest (chemical shifts), it is possible to determine the oxidation state and get information about bonding type for atoms in different materials (Skoog, et al. 1998).

2.2.6. Flame Atomic Absorption Spectrometry (AAS)

Spectroscopy is the measurement and interpretation of the electromagnetic radiation absorbed, scattered, or emitted by atoms or molecules. Interacting chemical species can be detected by spectroscopy because each species has a characteristic energy state.

Atomic absorption spectroscopy is based on the measurement of the absorption of resonance radiation by free atoms in the gaseous state, i.e. of spectral lines corresponding to the transition of atoms between the ground and excited states. Flame emission spectroscopy is a special area of emission spectroscopy in which a flame is used to excite the atoms. The components of a FAAS instrument is shown in the schematic diagram in Figure 2.4

In flame emission or absorption spectroscopy, the sample which is to be analyzed, usually an element concentration in the sample, is vaporized by an air-acetylene flame which will turn the aerosol sample into atoms in the ground state, some atoms will be exited above the ground state, those are minimal. Then a beam of radiant energy, a frequency which is that of the element in question, will pass though the flame and cause some of the ground state atoms to absorb energy and will create with the electronics a characteristic wavelength or resonance lines. The amount of radiant energy absorbed as a function of concentration of an element in the flame is the basis of atomic absorption spectroscopy.

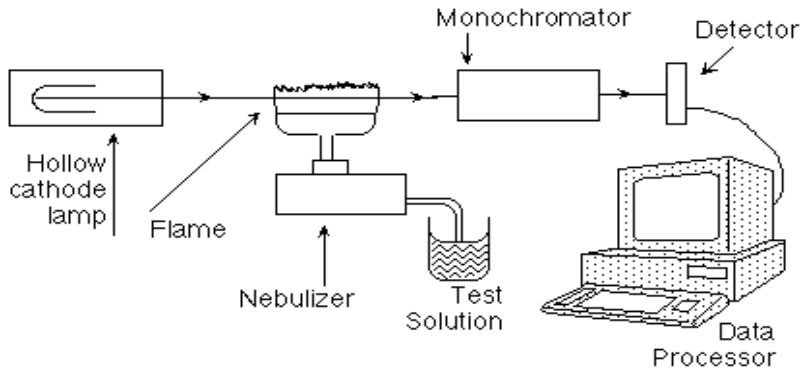

Figure 2.4. Schematic of Flame Atomic Absorption Spectrometry
(Source: New Mexico State University 2008)

2.3. Synthesis of nZVI

The synthesis of nZVI used in this work was done using borohydride reduction of Fe(II) (Wang and Zhang 1997, Wang, et al. 2006a). For this purpose, iron(II) chloride tetrahydrate ($FeCl_2.4H_2O$) and sodium borohydride ($NaBH_4$) were used. In each batch of synthesis, 1.50 g of Fe^{2+} (5.34 g $FeCl_2.4H_2O$) was dissolved in a 4/1 (v/v) ethanol/water mixture (24.0 ml ethanol + 6.0 ml deionized water) and stirred on a magnetic stirrer. On the other hand, 1.0 M sodium borohydride solution was prepared; 3.05 g $NaBH_4$ was dissolved in 100.0 ml of deionized water. The final BH_4^- / Fe^{+2} raito is adjusted to 3, since excess borohydride is needed for better growth of nanoparticles. The borohydride solution was poured in a burette, and then added dropwise to the Fe^{2+} solution, while still stirring on magntic stirrer. Black solid particles immediately appeared after the first drop of sodium borohydride solution. After adding the whole borohydride solution, the mixture was left for further 10 minutes of stirring.

The redox reaction can be represnted by :

$$Fe^{2+} + 2BH^- + 6H_2O \rightarrow Fe^0 + 2B(OH)_3 + 7H_2 \uparrow \quad (2.1)$$

Iron nanoparticles were separated from the liquid phase by,vacuum filtration, in which two sheets of blue band Whatman filter papers were used in each filtration process. At this point, the solid particles were washed at least three times with 25.0 ml portions of absolute ethanol to remove water. This washing process is probably the key step of synthesis since it prevents the rapid oxidation of zero-valent iron nanoparticles. The synthesized nanoparticles were finally dried in oven at 50^0 C overnight. Drying in evacuated ovens must be avoided because this would cause Fe nanoparticles to spontaneously ignite upon exposure to air.

2.4. Sorption Experiments

Throughout this study, the stock solutions of the cations were prepared with concentration of 5000.0 mg/L in 250 mL flasks. For Cd^{2+}, 2.54 g of $CdCl_2.2.5H_2O$, for Cu^{2+} 4.57 g of $Cu(NO_3)_2.2.5H_2O$, for Sr^{2+} 3.80 g of $SrCl_2.6H_2O$, for Zn^{2+} 5.70 g of

$Zn(NO_3)_2.6H_2O$, were dissolved in 250.0 ml of high purity water in a volumetric flask to yield 5000.0 mg/L stock solution of each ions and for Ni^{2+} 4.05g of $NiCl_2.6H_2O$, was dissolved in 250.0 ml of high purity water in a volumetric flask to yield 4000.0 mg/L stock solution. These solutions were used in preparing solutions with lower concentrations by serial dilution.

All the adsorption experiments were carried out at ambient temperature and pressure using 50.0 ml falcon tubes. The contents of the tubes were mixed on an orbital shaker operating at 350 rpm. After 4 hours of shaking (except for kinetic and desorption experiments), the tubes were centrifuged at 6000 rpm. The supernatant solutions were transferred into clean falcon tubes and acidified to 1% v/v with concentrated nitric acid. The solutions were kept in the fridge until analysis by AAS.

2.4.1. Effect of Contact Time

In the related experiments, 0.025 g of nZVI sample was added into 10.0 mL portions of 100.0 mg/L metal solutions, and the solutions were mixed for 10 min, 30 min, 1 h, 4h, 8 h, 24 h contact time. After centrifugation and acidification, supernantant solutions were kept in fridge until analysis.

2.4.2. Effect of Initial Metal Concentration

The effect of initial metal concentration on the extent of uptake were investigated at the initial cation concentrations of 10.0, 25.0, 50.0, 75.0, 100.0, 200.0, 300.0, 400.0, and 500.0 mg/L. The experiments were performed by adding 0.025 g, 0.050 g, or 0.10 g of nZVI sample into 10.0 mL potions of metal solutions (Ni^{2+} or Cd^{2+}). The mixtures were shaken on the orbital shaker for 4.0 hours and then removed for centrifugation. After centerifugation, the supernatant solutions were transfered into clean falcon tubes and concentrated nitric acid was added to these solutions to have a

final HNO_3 concentraiton of 1% (v/v). The solutions were kept in fridge until AAS analysis.

2.4.3. Effect of pH

The experiments were conducted after adjusting the initial pH's of the mixtures to 4.0, 6.0, 8.0, or 10.0 using 0.01 M, 0.1 M, or 1.0 M HNO_3 or NaOH. In each experiment 10.0 mL portions of metal solutions were contacted with 0.025 g nZVI for contact periods of 4.0 hours. After seperation of the liquid and solid phases by centrifugation, the solutions were acidified and kept in the fridge until analysis. The pH of the solutions were also measured at the the end of shaking process.

2.4.4. Desorption Studies

In order to assess the stability of adsorption, 10.0 mL portions of high purity water was added onto the cation-loaded nZVI and were shaken for 24 hours. After separation of liquid and solid phases by centrifugation, the solutions were acidified and kept in the fridge until analysis of the desorbed cation concentration.

2.4.5. Repetitive Application of nZVI

A series of repetitive experiments were performed to assess the reusability of nZVI materials in successive adsorption trials,. In each experiment 0.025 g nZVI doses were added into 10.0 mL aliquots of 10.0 mg/L or 100.0 mg/L metal solutions, in 50.0 mL falcon tube. After a shaking period of 30 minutes, the mixture were centrifuged, the supernatant solution were transfered into a clean tube and acidified. Then another 10.0 mL poriton of fresh metal solution possesing the same concentration as the previous portion was added onto the solid sample that remained in the tube. After a further

shaking time 30 minutes, the liquid phase was seperated again and kept for the analysis. These trails were repeated for seven times for each metal solution.

2.4.2. Effect of K^+ and Cs^+ on the Adsorption of Ni^{2+} and Cd^{2+} Ions

The effect of alkali and alkaline-earth metal cations on the extent of adsorption was studied using 100.0 mg/L solutions of K^+, and Cs^+as representative cations. In these experiments, 0.025 g nZVI sample doses were added into 10.0 mL potions of 10.0 mg/L, 25.0 mg/L, 50.0 mg/L, 75.0 mg/L, 100.0 mg/L metal solutions (Ni^{2+} or Cd^{2+}) containing K^+, or Cs^+, ion. The mixtures were shaken for 4.0 hours, and then removed for centrifugation. The supernatant solutions were then acidified and kept in fridge until analysis.

2.4.7. Comparative Uptake of Sr^{2+}, Zn^{2+}, and Cu^{2+} with that of Ni^{2+} and Cd^{2+} Ions

A series of experiments was perforem to compare the extent of uptake of Ni^{2+} and Cd^{2+} with those of Sr^{2+}, Zn^{2+}, and Cu^{2+} ions. These ions possess different values of reduction potential, and the aim of these experiment was to test the relation between the extent of adsorption and the reduction potential of the ions. The adsorption capacity experiments were studied at the initial cation concentrations of 10.0, 25.0, 50.0, 75.0, 100.0, 200.0, 300.0, 400.0, and 500.0 mg/L, at nZVI dose of of 0.025 g and 10.0 mL potions of metal solutions. The obtained results are discussed in section 3.8.

CHAPTER 3

RESULTS AND DISCUSSION

3.1. Characterization of nZVI

The nZVI samples synthesized and used in this study were characterized by different techniques in order to elucidate its elemental content, structural features, morphology, iso-electric-point, surface area, and particle size distribution in aqueous medium.

The XRD diagrams of fresh and aged nZVI samples are given in Figure 3.1. The figure indicates that freshly produced iron is in its Fe^0 state, characterized by the basic reflection appearing at 2 theta of 44.9°. No signal for the iron oxides (hematite, Fe_2O_3 or magnetite, Fe_3O_4) was observed in the fresh samples. It must be noted here that the absence of iron oxide signals in XRD diagram does not indicate that it is totally absent in the sample, as the oxide layer was found to possess an amorphous nature (discussed in light of TEM analysis in this text) and its quantity is small (might be below the detection limit of XRD). The nZVI samples stored for several weeks showed weak iron oxide signals in their XRD patterns. These features became more distinct (2 theta of 36°) in nZVI samples aged for 2-3 months (Figure 3.1b).

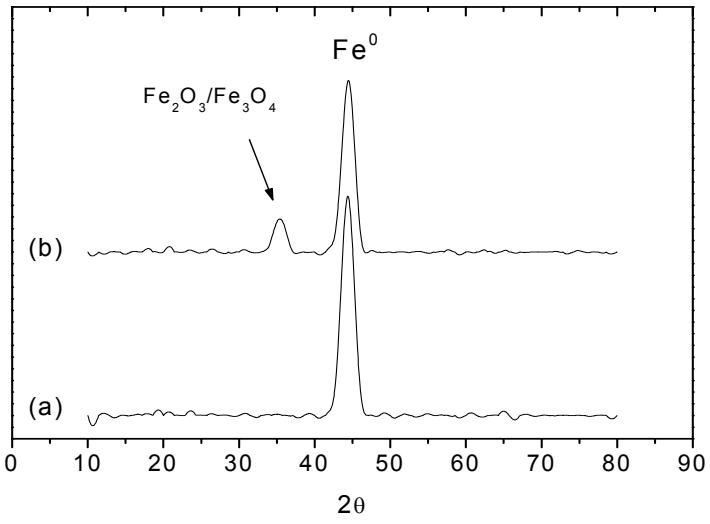

Figure 3.1. XRD patterns of nZVI; (a) fresh, and (b) 2 months after synthesis.

The presence of Fe and O in the surface of the nanoparticles is evident in the XPS spectrum given in Figure 3.2. XPS is a versatile surface sensitive technique that provides information about the upper ~ 10 nm of the surface. As shown in the figure, Fe presence is indicated by the Fe $2p_{3/2}$ and Fe $2p_{1/2}$ photoelectron peaks, while O is represented by the well-known O 1s peak in addition to O KLL Auger peak.

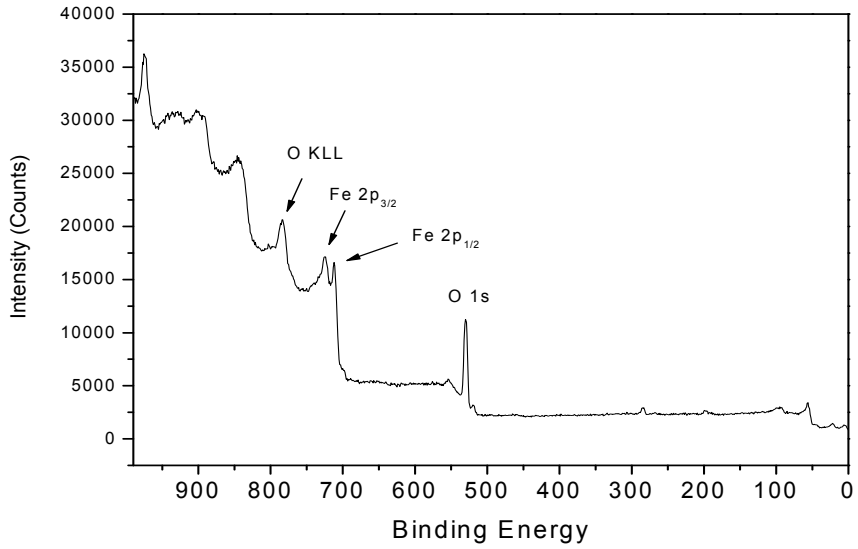

Figure 3.2. An XPS spectrum of a fresh sample of nZVI.

Typical SEM images of nZVI, shown in Figure 3.3, indicate the nanoparticles formed chain-like aggregates that can reach to several micrometers in length but are less than 100 nm in diameter. Aggregation of nanoparticles is reported to be caused by the large surface area and magnetic dipole-dipole interactions of the individual particles (Li, et al. 2006).

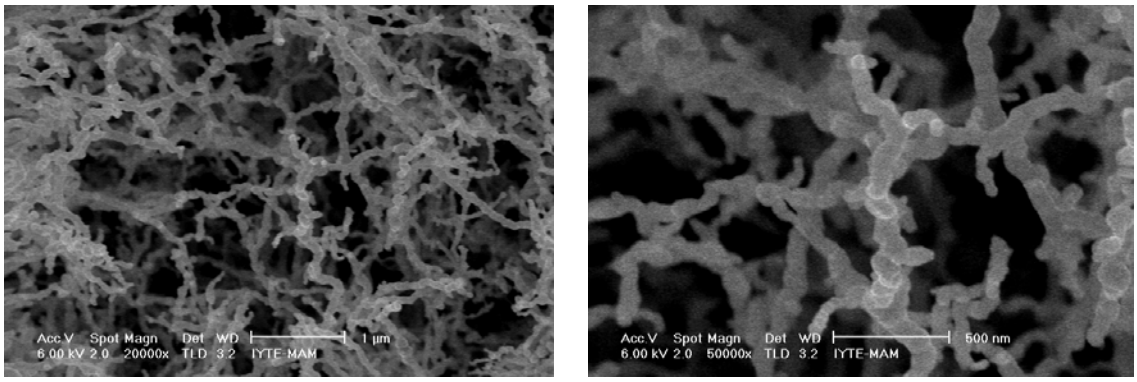

Figure 3.3. Typical SEM images of freshly prepared nZVI

The structure of nZVI was also analyzed using HR-TEM. Typical images are demonstrated in Figure 3.4. The nZVI particles appear in the characteristic chain-like structure, with the size of individual particles ranging within 20-60 nm. As is known, the exposure of nZVI to oxygen results in the development of an iron oxide layer, leading to a core-shell structure of the iron nanoparticles in which the core preserves the Fe^0 nature, while the core contains iron oxides (Fe_2O_3, Fe_3O_4, FeOOH) (Zhang 2003, Kanel, et al. 2006, Sun, et al. 2006). As Figure 3.4 reveals, the oxide layer appears to be about 2-3 nm thick, and the nanoparticles are thus dominated by iron in its zero-valent state. This oxide layer is thought to play an important role in the observed *slow* oxidation of iron nanoparticles by forming a barrier around the core. The oxide shell is considered to also provide a means for the transport of mass and charge across it in the solution medium (Kanel, et al. 2006, Li and Zhang 2007). Another important feature, as shown in Figure 3.4 images, is that the individual nanoparticles seem to be connected to each other in the chain-like structure via an 'oxide bridge'. As such, the oxide layer enhances the stability of the chain-like morphology. This morphology leads to decreasing the reactivity of the nanoparticles in terms of the available surface area, but at the same time provides the advantage of easier sorbent-solution phase separation at the end of adsorption operation.

The HR-TEM images showed high resolution lattice fringes in the core, indicating the presence of a crystalline Fe^0 phase. However, such fringes were not observed in oxide regions suggesting that the iron-oxide shell is highly amorphous. Similar results were reported earlier in the literature (Nurmi, et al. 2005).

HR-TEM investigations were also conducted on nZVI samples aged for different periods under atmospheric conditions. Typical HR-TEM image of an nZVI sample that was stored for about 6 months are shown in Figure 3.5. In general, iron nanoparticles retain their chain-like morphology (Figure 3.5a), with the thickness of the oxide layer showing variation within 5-10 nm (Figure 3.5b, 3.5c). However, regions occasionally appeared in which massive oxidation have taken place leading to a different morphology, and the oxide layer thickness was larger than 10 nm in nanoparticles with core-shell structure (Figure 3.5d).

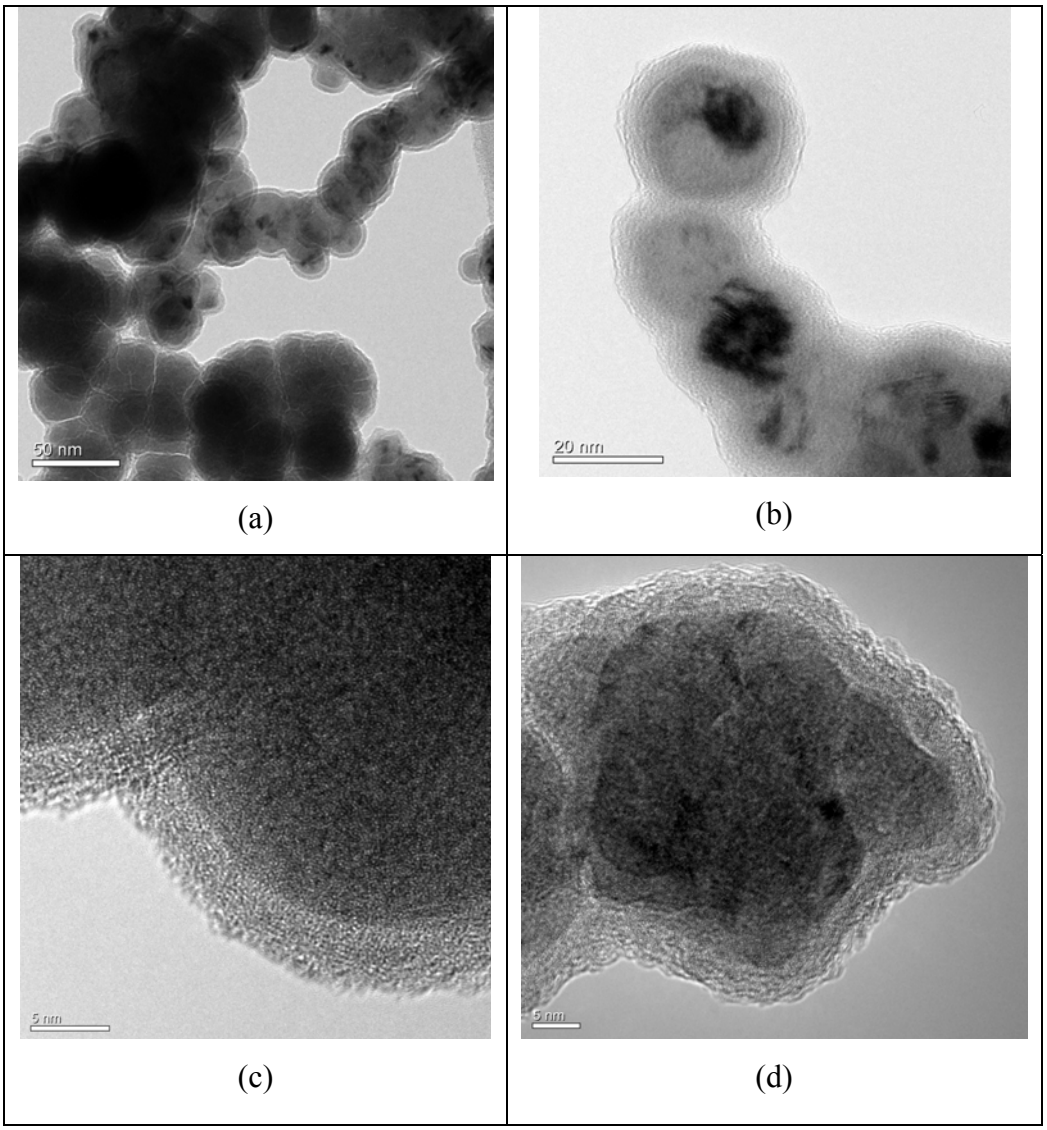

Figure 3.4. Typical HR-TEM images recorded at different magnifications for freshly prepared nZVI.

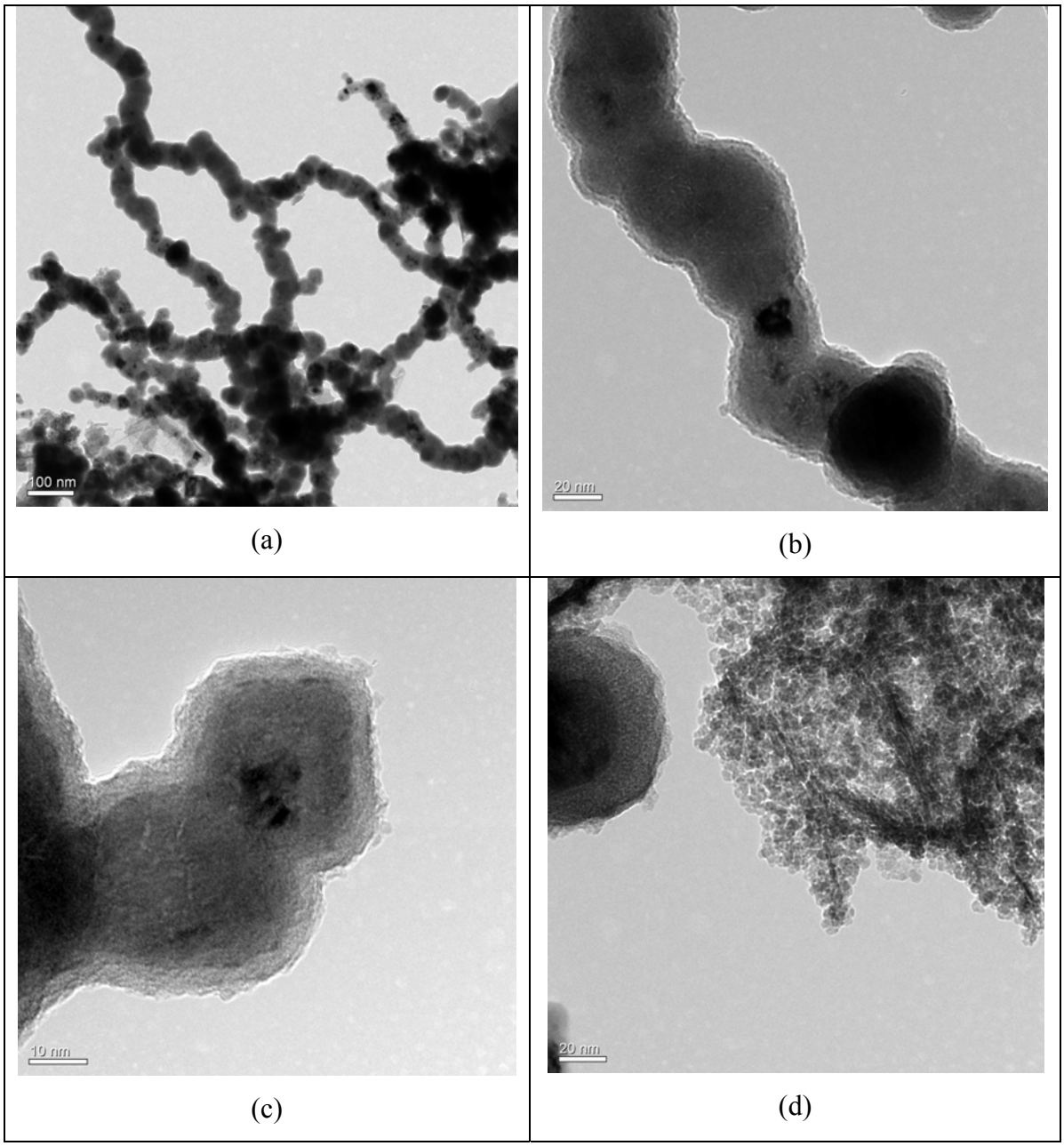

Figure 3.5. HR-TEM images recorded at different magnifications for nZVI aged for six months.

The zeta potential of nZVI aqueous suspensions was measured at different pH values to determine the Iso-Electric-Point (IEP) of the material. The results, The results, shown in Figure 3.6, indicate that the IEP occurred around 8.1-8.2.

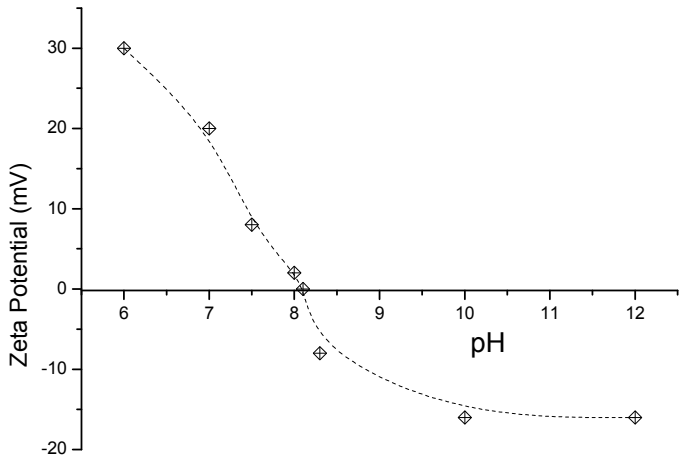

Figure 3.6. Values of Zeta Potential of nZVI at various pH's.

According to BET-N_2 analysis, the surface area was determined around 12-16 m^2 per g of iron nanoparticles. It is reported that a surface area measured on a dry basis is unlikely to reflect the actual available area in solution because of the tendency of nZVI particles to aggregate inside solution (Nurmi, et al. 2005).

3.2. Speciation of Metal Ions

In aqueous solution, transition metals are known to assume different chemical forms that depend on the pH of the medium. The speciation analysis of aqueous Ni^{2+} and Cd^{2+} ions was performed at various input conditions of initial concentration, temperature, pH, and ionic strength values using visual MINTEQ software. The obtained results for 100.0 mg/L concentrations are drawn in Figures 3.7 and 3.8. Both ions persist in their divalent forms up to pH value around 8. Beyond this, different hydroxyl forms of the two ions can be observed depending on the pH. These forms include $Ni(OH)^{+}$, $Ni(OH)_2$, $Ni(OH)_3^{-}$ for Ni, and $Cd(OH)^{+}$, $Cd(OH)_2$, $Cd(OH)_3^{-}$ and $Cd(OH)_4^{2-}$ for Cd. Within the pH ranges measured in the adsorption experiments of this study the two ions are expected to persist dominantly in their divalent forms.

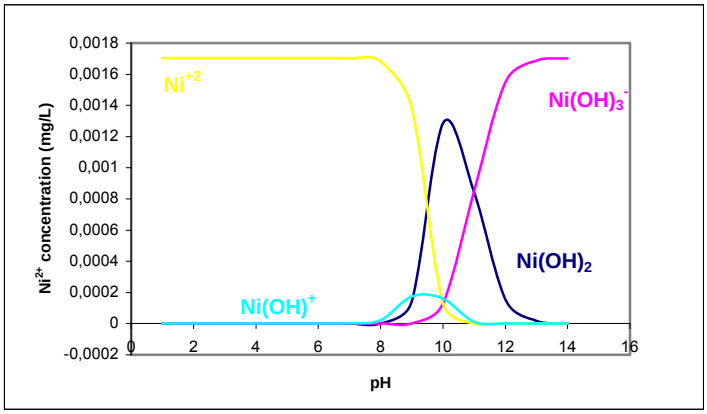

Figure 3.7. Speciation graph of Ni^{2+} ion at 100.0 mg/L

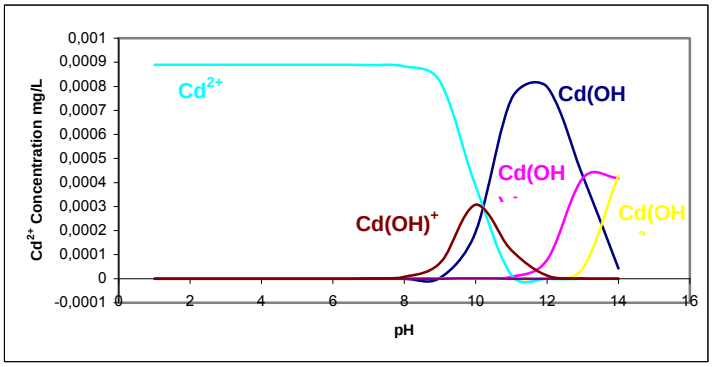

Figure 3.8. Speciation graph of Cd^{2+} ion at 100.0 mg/L

3.3. Effect of Time

The first set of experiments was performed to determine the time required to approach equilibrium upon contact of Ni^{2+} and Cd^{2+} ions with nZVI. These experiments were carried out as explained in section 2.4.1.. The obtained results, shown in Figure 3.9, indicate that the uptake approach equilibrium at nearly one hour of shaking time for both of the metals. The experiments in the next sections were performed at four hour mixing time in order to ensure the attainment of equilibrium.

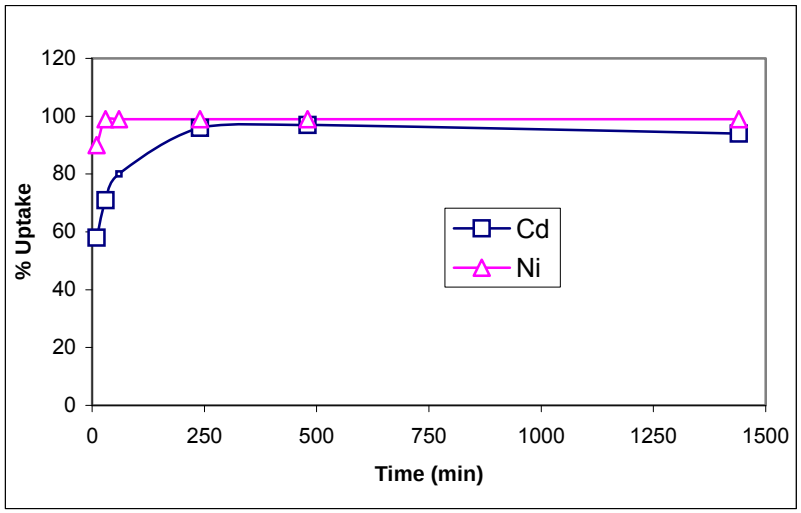

Figure 3.9. Variation of % uptake of Ni^{2+} and Cd^{2+} with contact time

Throughout this study, the equilibrium concentrations of Ni^{2+} and Cd^{2+} on nZVI were calculated using the well-known mass balance equation:

$$[C]_s = ([C]_0 - [C]_l) \times (V/M) \qquad (2.2)$$

Where $[C]_s$ is the concentration of Ni^{2+} or Cd^{2+} on nZVI (mg/g), $[C]_l$ is their concentration in liquid solution (mg/L), V is the solution volume (L), and M is the mass of nZVI (g).

3.4. Effect of Initial Concentration at Different nZVI Doses

These experiments were performed according to the procedure mentioned in section 2.4.2. The variation in the extent of uptake as a function of initial concentration at three different doses of nZVI is shown in Figure 3.10 for Ni^{2+} and in Figure 3.11 for Cd^{2+} ions. The amounts of tried nZVI samples were 0.025 g, 0.050 g, or 0.10 g added into 10 mL potions of metal solutions. This correspond to nZVI concentrations of 2.5, 5.0, and 10.0 g/L. For both ions, a complete removal of both ions is acheivable at all doses up to the initial concentration of 100.0 mg/L. Beyond this concentration a complete removal can still be acheived by increasing the nZVI amount. According to the graph of Ni^{2+}, the amount of 0.025 g nZVI yield identical results as those obtained at 0.050 g amount. On the overall, the percentages of uptake for Ni^{2+} appear to be larger than those for the Cd^{2+} ions. The priority of uptake is discussed in the context of the uptake mechanism in section 3.8.

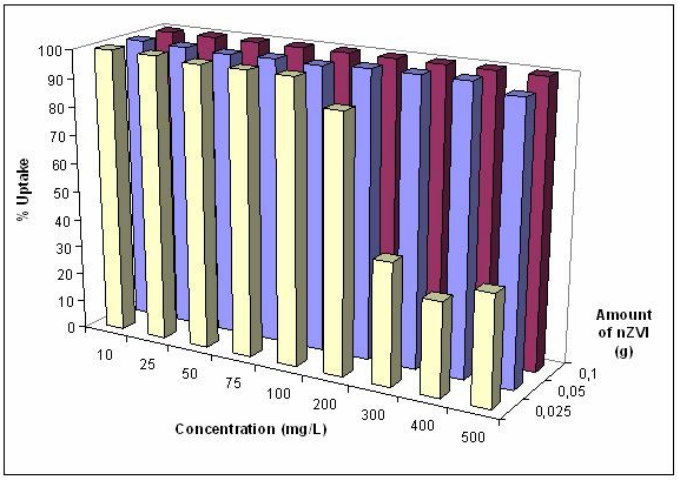

Figure 3.10. Variation of % uptake of Ni^{2+} with initial concentration and amount of applied nZVI

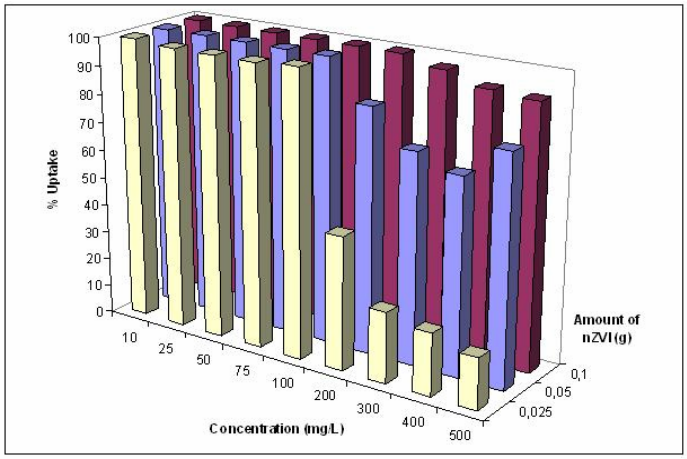

Figure 3.11. Variation of % uptake of Cd^{2+} with initial concentration and amount of applied nZVI

3.5. Desorption Analysis

The aim of the desorption studies was to assess the stability of adsorption. For this purpose, nZVI samples pre-loaded with Ni^{2+} or Cd^{2+} were shaken into ultra pure water for 24 hours. The solutions were then analyzed for their Ni or Cd contents by AAS. The results are shown in Tables 3.1 and 3.2 for Ni^{2+}, and in Tables 3.3 and 3.4 for Cd^{2+} ions. As is seen in the tables, almost no desorption occurs from samples loaded with initial concentrations below 200.0 mg/L, indicating a high stability of adsorption for both ions within the given range of concentrations. Beyond this, partial desorption is observed. This is probably pointing to the presence of a second (less favorable) type of adsorption sites or mechanism with limited adsorption capacity that become operative at higher metal concentrations. For both ions, the increase in nZVI amount causes less desorption as it increases the possibility of cations to be fixed by more favourable sites.

Table 3.1. Desorption for Ni^{2+} pre-loaded on nZVI at different initial concentrations and 0.025 g of nZVI

Initial Conc. (mg/L)	**[C]s mg/g from sorp. data**	***[C]l mg/L *(for 100% desorption)***	**[C]l mg/L Measured Desorped Conc.**	**% Desorp.**
10.0	4	10	0	0
25.0	10	25	0	0
50.0	20	50	0	0
75.0	30	75	0	0
100.0	40	100	0	0
200.0	72	179	2	1
300.0	51	128	26	20
400.0	52	131	30	23
500.0	77	193	49	25

Table 3.2. Desorption for Ni^{2+} pre-loaded on nZVI at different initial concentration and 0.050 g of nZVI

initial conc. (mg /L)	**[C]s mg/g from sorp. data**	***[C]l mg/L *(for 100% desorption)***	**[C]l mg/L Measured Desorped Conc.**	**% Desorp.**
10.0	2	10	0	0
25.0	5	25	0	0
50.0	10	50	0	0
75.0	15	75	0	0
100.0	20	99	0	0
200.0	40	200	3	2
300.0	60	300	9	3
400.0	80	400	48	12
500.0	97	485	103	21

Table 3.3. Desorption for Cd^{2+} pre-loaded on nZVI at different initial concentration and 0.025 g of nZVI

initial conc. (mg/L)	**[C]s mg/g from sorp. data**	***[C]l mg/L *(for 100% desorption)***	**[C]l mg/L Measured Desorped Conc.**	**% Desorp.**
10.0	4	10	0	0
25.0	10	25	0	0
50.0	20	50	0	0
75.0	30	75	0.5	<1
100.0	40	100	0.6	<1
200.0	38	94	8	9
300.0	30	75	36	48
400.0	35	88	31	35
500.0	31	78	37	47

Table 3.4. Desorption for Cd^{2+} pre-loaded on nZVI at different initial concentration and 0.050 g of nZVI

İnitial conc. (mg/L)	**[C]s mg/g from sorp. data**	***[C]l mg/L *(for 100% desorption)***	**[C]l mg/L Measured Desorped Conc**	**% Desorp.**
10.0	2	0	0	0
25.0	5	0	0	0
50.0	10	0	0	0
75.0	15	0	0,3	0
100.0	20	0	0	0
200.0	34	172	6	3.5
300.0	44	221	43	19.5
400.0	55	277	42	15
500.0	80	399	59	15

3.6. Effect of pH

The effect of pH on the removal of Ni^{2+} and Cd^{2+} by nZVI was studied under the conditions described in section 2.4.3. The obtained results expressed as concentrations on the solid (mg/g) and percentage adsorption at different pH values and nZVI amounts are given Table 3.1 for Ni^{2+} and in Table 3.2 for Cd^{2+}. As is sees, for the studied concentration, there is no significant change in the amounts of removed metal ions which appears to almost go to completion at different pH values. This is indicative that the adsorption of the cations at the studied concentration is not dependent on the protonation/deprotenation reactions on the surface of iron nanoparticles. As noted previously in this text, the IEP of nZVI was around 8.1-8.2. Hence, at pH values below the IEP, the surface is expected to possess a positive potentials that restrict the interaction of the cations with the sorbent. As the pH is increased beyond the IEP of the sorbent, the surface potential became negative and the resulting attractive forces shrank the double layer leading to a higher chance of sorbate-sorbent interaction. However, in the cases of Ni^{2+} and Cd^{2+}, the pH seems to be not affecting the uptake, the thing that indicates that the mechanism of adsorption is independent on the surface charge. This conclusion, however, has to be verified over a wide range of concentrations.

Table 3.5 The equilibrium values corresponding to the uptake of Ni^{2+} ion by nZVI at various initial solution pH values

pH	0.025 g nZVI / 100 mg/L			0.05 g nZVI / 100mg/L			0.1 g nZVI / 100 mg/L		
	$[C]_l$ mg/L	$[C]_s$ mg/g	% Ads	[C]l mg/L	[C]s mg/g	% Ads	[C]l mg/L	[C]s mg/g	% Ads
4.0	16	34	84	0,4	20	>99	0	10	>99,9
6.0	9	36	91	0,8	20	>99	0	10	>99,9
8.0	0	40	>99,9	0	20	>99,9	0	10	>99,9
10.0	0	40	>99,9	0	20	>99,9	0	10	>99,9

Table 3.6 The equlibrium values corresponding to the uptake of Cd^{2+} ion by nZVI at various initial solution pH values

pH	0.025 g nZVI / 100 mg/L			0.05 g nZVI / 100mg/L			0.1 g nZVI / 100 mg/L		
	[C]l mg/L	[C]s mg/g	% Ads	[C]l mg/L	[C]s mg/g	% Ads	[C]l mg/L	[C]s mg/g	% Ads
4.0	0,5	40	**>99**	0,5	20	**>99**	0,5	10	**>99**
6.0	0,6	40	**>99**	0,5	20	**>99**	0,5	10	**>99**
8.0	0,6	40	**>99**	0,6	20	**>99**	0,5	10	**>99**
10.0	0,5	40	**>99**	0,6	20	**>99**	0,6	10	**>99**

3.7. Repetitive Loading

Since Fe based materials are susceptible to oxidation in a wet environment, other sets of experiments were conducted to evaluate the effect of repetitive application of an nZVI sample on its capability extent of removal of Ni^{2+} and Cd^{2+} ions. The related experiments were performed under the conditions described in section 2.4.5, and the obtained results are shown in Figure 3.14 for Ni^{2+} and 3.15 for Cd^{2+}.

The results obtained for two different nZVI doses indicate that the reusability is concentration dependent for both cations. While in the case of Ni^{2+}, the sorbent capability for adsorption is largely deteriorated after the first application, in Cd^{2+} case multiple use of the same nZVI seems to be possible in particular at lower concentrations. This could be pointing to differences in the adsorption mechanisms of the cations. The results provide an extra advantage for nZVI application in Cd^{2+} removal.

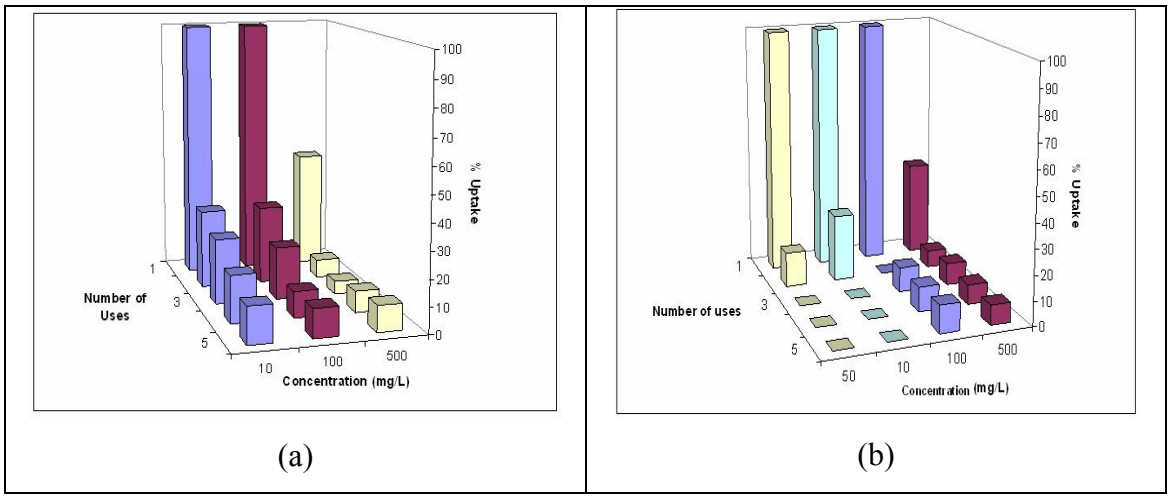

Figure 3. 12. Variation of % uptake of Ni^{2+} with number of repetetive uses of nZVI sample; (a) amount of nZVI is 0.025 g, (b) amount of nZVI is 0.050 g

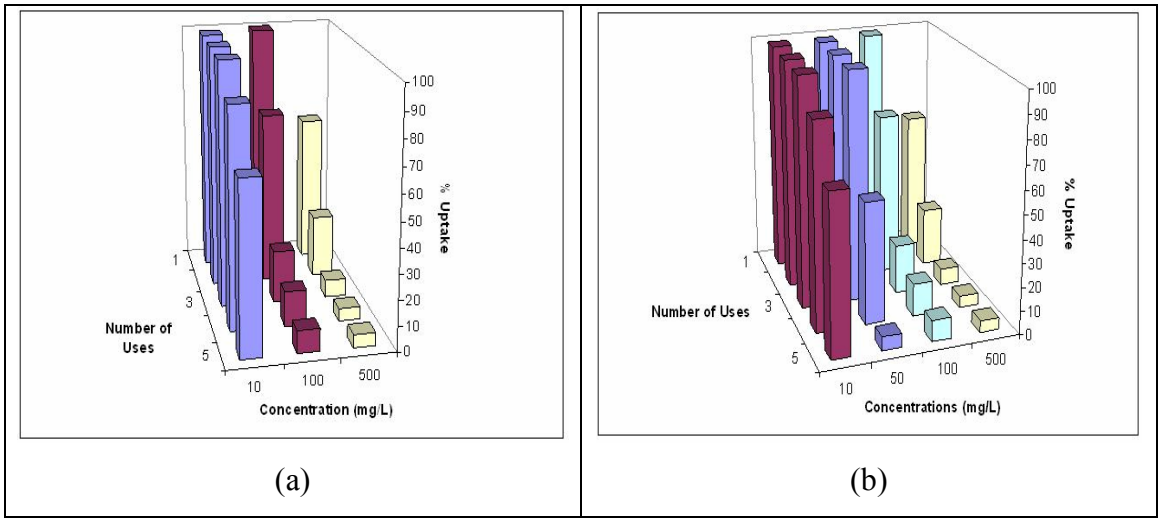

Figure 3.13. Variation of % uptake of Cd^{2+} with number of repetetive uses of nZVI sample; (a) amount of nZVI is 0.025 g, (b) amount of nZVI is 0.050 g

3.8. Competetive Effects of K^+ and Cs^+ Ions on Ni^{2+} and Cd^{2+} Uptake Effect of Competing Ions

Group I cations are widely abundant in water media. For this reason, K^+ and Cs^+ were selected as representative for the mentioned group and their competitive effect on the uptake of Ni^{2+} and Cd^{2+} was studied over a wide range of cation concentrations.

Table 3.7: Effect of K^+ and Cs^+ ion on the uptake of Ni^{2+} for 0.1 g nZVI

initial conc. (mg /L)	100 mg/L K^+			100 mg/L Cs^+		
	[C]l mg/L	% Ads of Ni^{+2}	% Ads of K^+	[C]l mg/L	% Ads of Ni^+	% Ads of Cs^+
10.0	~0	>99.9	15	~0	>99.9	8
25.0	~0	>99.9	11	~0	>99.9	7
50.0	~0	>99.9	9	~0	>99.9	7
75.0	~0	>99.9	7	~0	>99.9	6
100.0	~0	>99.9	4	~0	>99.9	5

Table 3.8: Effect of K^+ and Cs^+ ion on the uptake of Cd^{2+} for 0.1 g nZVI

initial conc. (mg/L)	100ppm K^+			100ppm Cs^+		
	[C]l mg/L	% Ads of Cd^{+2}	% Ads of K^+	[C]l mg/L	% Ads of Cd^{+2}	% Ads of Cs^+
10.0	1	99	12	~0	>99.9	10
25.0	1	99	13	~0	>99.9	8
50.0	1	99	9	~0	>99.9	7
75.0	1	99	6	~0	>99.9	5
100.0	1	99	5	~0	>99.9	2

The experimental conditions under which the related experiments were carried out are described in section 2.4.6.. The obtained results are given in Table 3.7 for Ni^{2+} and in Table 3.8 for Cd^{2+}. As can be seen from the tables , both of K^+ and Cs^+ ions did not effect the percentage adsorption of Ni^{2+} and Cd^{2+} ions at different initial concentrations. The tables show also that only minimal amounts of K^+ and Cs^+ ions were fixed by the nZVI samples. These results goes in line with our previous findings that showed that nZVI had small affinity towards K^+ in solutions of Cu^{2+} (Karabelli et al., 2008). In the same study, it was also shown nZVI has low affinity for the group II cations Mg^{2+} and Ca^{2+}, the thing that is also confirmed in this study for Sr^{2+} as discussed in the next section.

3.9. Mechanism of Uptake

The uptake mechanisms demonstrated by iron nanoparticles towards sorbed metallic ions are connected with the core-shell structure of the nanoparticles. These mechanisms include reduction of the ions by Fe^0 present in the core of the nanoparticle, electrostatic adsorption or complex formation to the oxohydroxyl groups (FeOOH) on the shell surface, in addition to precipitation (Li and Zhang 2007). The contribution of each of these mechanisms can vary with the standard electrode potential of the sorbate ion, its charge density, and the operating experimental conditions, in particular pH of the medium in comparison with the iso-electric point (IEP) of nZVI surface.

The core, constituted of zero-valent iron, forms an electron source that might reduce ions possessing higher standard reduction potential than iron. It is proposed that electron transfer from Fe^0 to the incoming cation, when equilibrium is established, might take place mainly via one of the following routes (Li and Zhang 2007):

1. Direct electron transfer from the core through the defects in the oxide shell to the incoming cation,
2. Indirect electron transfer from the core through the conduction band of the oxide shell to the incoming cation. For such a transfer to be thermodynamically favorable the energy of the electrons in the iron metal and/or the oxide layer must be more negative than the standard potential of the redox couple of the incoming cation.

As a result, unless a direct electron transfer is taking place (the extent of which is unclear), the redox process will be governed by the Fermi energy (E_F) of the oxide shell, the value of which is reported to vary between -0.18 to -0.33 V (Balko and Tratnyek 1998). A simplified band diagram of the iron/iron oxide/aqueous metal cations at pH 7 is shown in Fig. 3.14. The figure shows the values of the Fermi energies, E_F, for iron and iron oxide in addition to the energies of the conduction band, E_{CD}, and the valence band, E_{VB}, in the oxide shell. The reduction potential for a number of ions is also labelled on the diagram, and additionally the reduction potentials of the elements investigated in this study are also given in Table 3.7.

It is expected that cations that possess standard reduction potential larger than that of Fe^{2+} (= -0.44 V, 298 K) will undergo reduction by Fe^0 if such cations have a direct physical contact with the Fe^0 surface. However, the presence of iron oxide shell

around the Fe^0 core in iron nanoparticles brings about a further restriction. In this case, it is necessary for cations to possess reduction potentials that are more positive than the energy of the conduction band of iron oxide in order to receive electrons supplied by Fe^0 through the conduction band of the oxide.

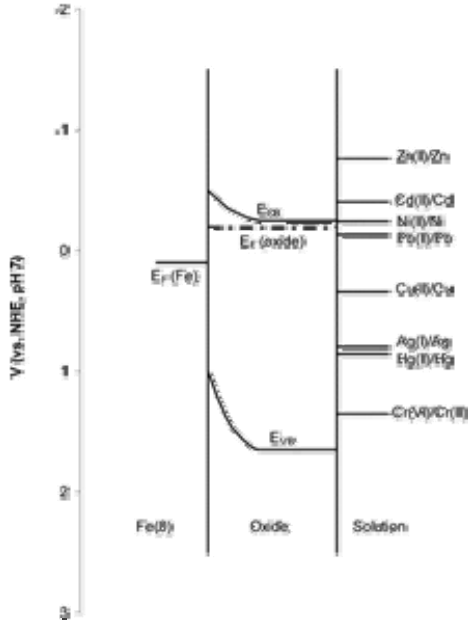

Figure 3.14. A simplified band diagram of the iron/iron oxide/aqueous metal cations at pH 7. (Source: Li and Zhang 2007)

Table 3.9. Standard Electrode Potentials at 25 °C

Element	Half-Cell Reaction	E^0 (V)
Strontium (Sr)	$Sr^{2+} + 2\ e^- \rightarrow Sr$	-2.89
Zinc (Zn)	$Zn^{2+} + 2\ e^- \rightarrow Zn$	-0.76
Iron (Fe)	$Fe^{2+} + 2\ e^- \rightarrow Fe$	-0.44
Cadmium (Cd)	$Cd^{2+} + 2\ e^- \rightarrow Cd$	-0.40
Nickel (Ni)	$Ni^{2+} + 2\ e^- \rightarrow Ni$	-0.23
Copper (Cu)	$Cu^{2+} + 2\ e^- \rightarrow Cu$	0.34

Literature resources have reported redox mechanisms for a number of cations by nZVI; e.g. Pb^{2+} and Cr^{6+} (Ponder, et al. 2000), As^{3+} and As^{5+} (Kanel, et al. 2005; Kanel, et al. 2006), and Cu^{2+} (Karabelli, et al. 2008), Ag^{+} (Li and Zhang 2007). What is common among these ions is the fact that they possess standard reduction potentials well above that of iron and more positive than the energy of the conduction band of iron oxide shell. However, the reduction process was not confirmed for ions with standard reduction potential that is only slightly above that of iron like Co^{2+} .(Üzüm, et al. 2008) and Cd^{2+} (Li and Zhang 2007), which were reported to be sorbed on the external surface hydroxyl groups of the iron oxide shell. In cases where the reduction potential of the metal cation (Me^{2+}) is not higher enough than that of Fe^{0}, it is thought that the unoccupied electron energy levels of the cation will not be able to undergo effective overlap with the conduction band of the oxide shell to produce Me^{0}, due to the high E_F value of the oxide shell in comparison to the reduction potential of such cations (Li and Zhang 2007). In this case, the cation will be attached by the exposed oxohydroxyl groups at the interface of the oxide shell and the solution without being reduced.

From Fig. 3.14 it is clear that the reduction potential of Cd^{2+} is smaller than the energy of the conduction band, E_{CD}, of the oxide shell. Thus reduction of Cd^{2+} ions by nZVI is theoretically implausible. The XPS surveys confirmed that metallic Cd was not present after sorption on nZVI, which is in line with a result reported recently in literature (Li and Zhang 2007). In addition, the XPS surveys indicated the possibility of $Cd(OH)_2$ formation on the nZVI sample loaded with Cd^{2+} solutions at 500 mg/L initial concentration.

For Ni^{2+} ions the situation is ambiguous. As seen from Figure 3.14, the reduction potential of Ni^{2+} larger than that of Fe^{2+}, but is very close to the energy of the conduction band, E_{CD}, of the oxide shell. The reduction of partial amounts of Ni^{2+} by nZVI was reported in literature in line with fixation of the ion by oxohydroxide groups on the surface of iron nanoparticles (Li and Zhang 2006). However, in our XPS investigations, the reduction of Ni^{2+} was not confirmed. A typical XPS spectrum of nZVI after Ni^{2+} uptake is shown in Figure 3.15. The inset in the figure shows the Ni 2p peaks in the samples. As reported in literature, the binding energy of metallic nickel Ni^{0} is well known to occur at 852.8 ± 0.2 eV for the Ni $2p_{3/2}$ line (Wagner, et al. 1979 ; Kishi and Fujita 1990). The binding energy of the Ni $2p_{3/2}$ line reported for Ni^{2+} in NiO is 854.4 ± 0.2 eV (Wagner, et al. 1979 ; Kishi 1988), and for the Ni^{3+}-based oxide Ni_2O_3 the Ni $2p_{3/2}$ line is reported at 856.0 eV (Kishi 1988 ; Salvati, et al. 1981). For nickel

hydroxide; $Ni(OH)_2$, the reported binding energy of the Ni $2p_{3/2}$ line shows some variation in the literature, from 855.6 eV (McIntyre and Cook 1975 ; Lorenz, et al. 1979) to 856.0 eV (Li and Hercules 1984), occurring at a similar binding energy to that reported for Ni_2O_3.

In the current study, the Ni $2p_{3/2}$ peak was recorded at a binding energy centre of 855.95 ± 0.1eV which is far enough from that of metallic Ni, and corresponds most closely to values previously reported for $Ni(OH)_2$. The overall analysis points to the possibility of fixation of Ni^{2+} ions by oxohydroxide groups at the surface-solution interface in addition to precipitate formation at high Ni^{2+} concentrations, but no signs of reduction were observed.

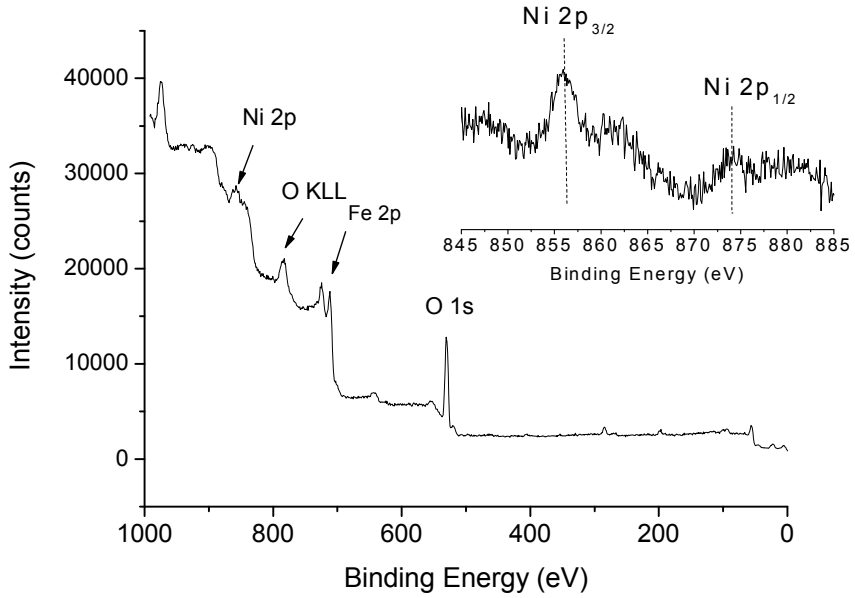

Figure 3.15. A typical XPS spectrum of nZVI after Ni^{2+} uptake. The inset in the figure shows the Ni 2p peaks in the samples

The XPS results indicate also that the iron nanoparticles had undergone wet oxidation to form iron hydroxides (essentially rust). The O 1s photoelectron profile displayed a peak centred at 530.7 ± 0.1 eV that was slightly asymmetric to the high binding energy side. Curve fitting of the O 1s profile indicated three peaks contributed

to the overall signal, centred at 530.0 eV, 531.3 eV and 532.9 eV respectively. The predominant signal contribution (peak 1) was attributed to O^{2-} in metal oxides (44%) with a similar contribution (40% by area) attributed to structural OH^- in solid hydroxide phases (peak 2); either $Ni(OH)_2$ or FeO(OH). The peak fitted at 532.9 eV was characteristic of physi-sorbed water and accounted only to 16% of the signal contribution. The binding energy values previously reported for the O 1s line recorded from $Ni(OH)_2$ are typically in the range of 531.2 eV (Lorenz, et al. 1979 ; Löchel and Strehblow 1984) to 531.7 eV (Kishi and Ikeda 1973 ; Kim and Winograd 1974). The recorded Fe 2p photoelectron profiles for both samples was very similar to that previously reported for Fe in iron oxohydroxide (FeOOH) (Kishi and Fujita 1990 ; Lorenz, et al. 1979) with the Fe $2p_{3/2}$ line centred at 711.6 ± 0.1eV binding energy.

Typical HR-TEM images of iron nanoparticles after being exposed to Ni^{2+} and Cd^{2+} solutions are shown in Fig. 3.16. The images indicate enhanced oxidation of iron nanoparticles, the extent of which is pronounced more in the case of exposure to Ni^{2+} ions. This exposure is seen to affect also the morphology of iron nanoparticles.

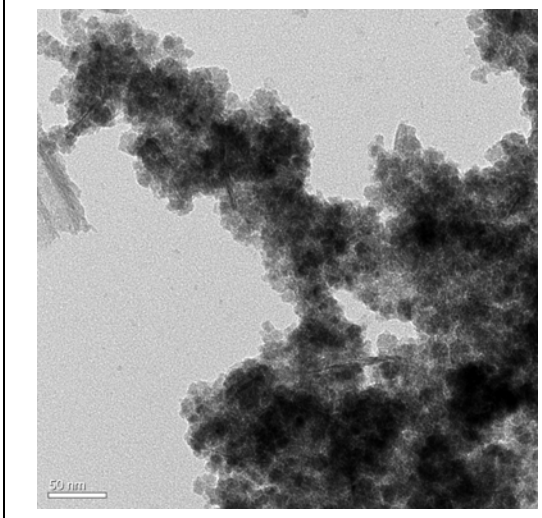

(a)

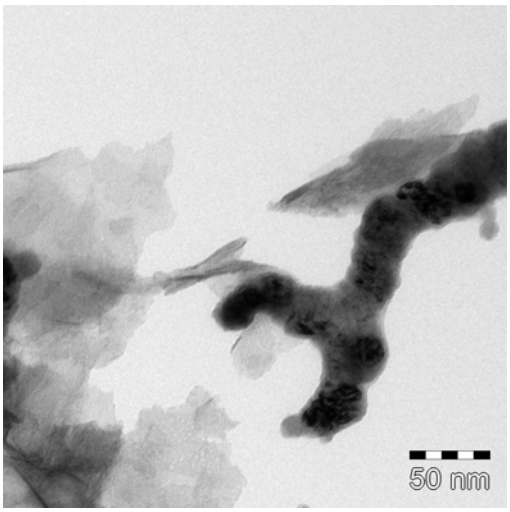

(b)

Figure 3.16. Typical HR-TEM images of iron nanoparticles after being exposed to: (a) Ni^{2+}, and (b) Cd^{2+} solutions.

Further experiments were performed to compare the extent of retention of Ni^{2+} and Cd^{2+} to those of Sr^{2+}, Zn^{2+}, and Cu^{2+} which possess different values of reduction potentials (see Table 3.9). The related experiments attempted to elucidate any possible correlations between the standard reduction potential of these ions and their extent of uptake. For Sr^{2+}, the standard reduction potential is much smaller than that of Fe^{2+} and thus its reduction by nZVI is not expected. Cu^{2+}, on the other hand, possesses a standard reduction potential well above that of Fe^{2+} and its reduction was documented in a previous study carried out at our laboratories (Karabelli, et al. 2008). The standard reduction potential of Zn^{2+} is below that of Fe^{2+}, but it has a charge density (charge/size) close to those of Ni^{2+} and Cd^{2+} ions. The sizes of the ions are provided in Table 3.10.

Table 3.10. The radii of cations (Shannon Radii) at their smallest and highest coordination numbers (CN)

Cation	**Radius (pm)**
Sr^{2+}	118 at CN of VI 144 at CN of XII
Ni^{2+}	55 at CN of IV 69 at CN of VI
Cu^{2+}	57 at CN of IV 73 at CN of VI
Zn^{2+}	60 at CN of IV 90 at CN of VIII
Cd^{2+}	78 at CN of IV 131 at CN of XII

The investigations included the effects of time, concentration, in addition to some desorption tests. The results of the kinetic experiments are shown in Figure 3.17. Equilibrium is achieved very rapidly for all ions except for Sr^{2+} for which sorption continued to increase over the studied period. The exceptional behavior of Sr^{2+} persists also when the effect of concentration is studied. The experiments were performed within the range of 10.0-100.0 mg/L initial concentrations and the results of which are given in Table 3.11. According to the data, Sr^{2+} ions appear as the least preferred ones

by nZVI. As is known, Sr^{2+} is different from the remaining ions in being a group II cation while the others belong to transition metals block.

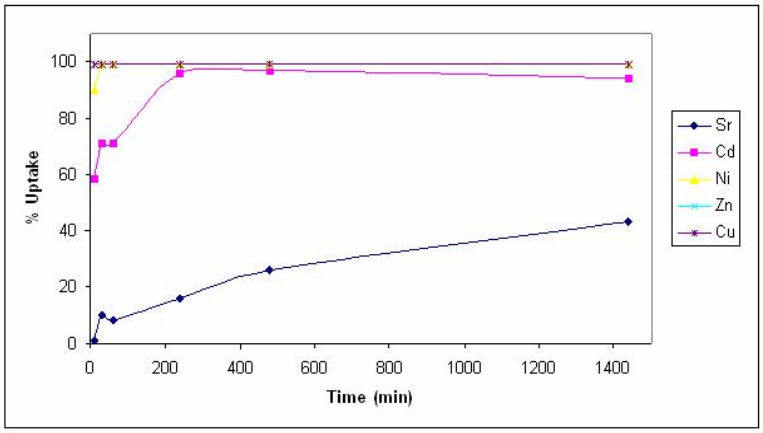

Figure 3.17. Effect of time on the uptake of different ions at initial concentration of 100.0 mg/L.

Table 3.11. Effect of initial cation concentration on the **%** uptake of various cations by nZVI

Initial Conc. (mg/L)	**% Uptake**				
	Cd^{2+}	**Ni^{2+}**	**Zn^{2+}**	**Cu^{2+}**	**Sr^{2+}**
10.0	>99.9	>99.9	>99.9	>99.9	77
25.0	99	99.6	>99.9	>99.9	40
50.0	99	99	>99.9	>99.9	44
75.0	99	99	99	>99.9	52
100.0	95	99	70	>99.9	43

The principal reason for the difference is most plausibly the significantly lower charge density of Sr^{2+} in comparison with the others. The charge density is an important factor to look at when complexation reactions (or inner-sphere complex formation between sorbed cation and hydroxide groups on the surface of iron nanoparticles) are considered. According to the results in Table 3.11 within the given range of

concentration, the priority of fixation of the studied cations by nZVI follows the order: $Cu^{2+} > Ni^{2+} > Cd^{2+} > Zn^{2+} > Sr^{2+}$.

Here it must be stressed that the difference in % uptake between the four transitions metal ions is not significant up to the initial concentration of 100.0 mg/L at which some differences are observed. This might be referred to the resemblance of chemical nature among these ions and relatively close charge densities. It is interesting to note also that the priority order follows the standard reduction potential of the cations. The same priority was, however, not obeyed when further experiments were performed at higher initial concentrations of the cations. The results, given in Table 3.12 indicate that the highest uptake is achieved in the case of Ni^{2+} ions and that the uptake of Zn^{2+} becomes comparable to that of Cd^{2+} and Cu^{2+} ions which possess higher standard reduction potentials than Zn^{2+} ions.The decrease in Cu^{2+} retention at higher concentrations migth be attributed to the formation of Cu_2O and Cu^0 on the surface of nZVI, in a way that restricts the interaction of further Cu^{2+} ions with nZVI surface (Karabelli et al. 2008).

Table 3.12. Effect of higher initial cation concentrations on the **%** uptake of studied transition metal cations by nZVI

Initial Conc. (mg/L)	**% Uptake**			
	Cd^{2+}	**Ni^{2+}**	**Zn^{2+}**	**Cu^{2+}**
200.0	47	90	60	65
300.0	25	43	20	42
400.0	22	33	15	23
500.0	18	39	16	16

Under the given circumstances, it seems that the charge density of the cation becomes increasingly effective in determining the extent of uptake as the initial concentration is raised. This might be related with the better ability smaller cations to diffuse and form inner-sphere complexes (binding of cations to inner oxygen atoms in oxohydroxyl groups in the oxide shell).

The desorption behavior of the cations was also studied in order to test the stability of uptake and the obtained results are provided in Table 3.13 The results indicate that Sr^{2+} uptake is highly unstable in particular for nZVI samples pre-loaded

with high initial concentrations. On the other hand, the uptake of the four transition metal cations appears to be very stable, with only minimal amounts released at the end of the desorption period (24 hours).

Table 3.13. The % desorption of studied cations loaded previously on nZVI at different initial concentrations

Initial Conc. (mg/L)	**% Desorption**				
	Cd^{2+}	**Ni^{2+}**	**Zn^{2+}**	**Cu^{2+}**	**Sr^{2+}**
10.0	0	0	0	0	63
25.0	0	0	0	0	60
50.0	0	0	0	0	41
75.0	<1	0	0	0	28
100.0	<1	0	0	0	33
200.0	9	1	3	0	35
300.0	48	20	7	0	16
400.0	35	23	10	0	15
500.0	47	25	10	0	16

It is worth noting that Cu-nZVI samples demonstrated the highest stability among the studied cations, the thing that might be due to the oxidation-reduction mechanism in the case of Cu^{2+} uptake that leads to irreversible transformation of Cu^{2+} ions into metallic Cu. For the other transition metals for which the oxidation-reduction mechanism is implausible, the high stability of sorption is confirming the presumable inner-sphere complex formation as the sorption mechanism. In the case of Sr^{2+}, however, the high reversibility of sorption is indicative that the ion is fixed to nZVI surface through outer-sphere complex formation, i.e. weak electrostatic attractions.

CHAPTER 4

CONCLUSION

In this study, nanoscaled zero-valent iron (nZVI) (20-80 nm) was synthesized in ethonal by borohydride-reduction method under atmospheric conditions. The nanoparticles were composed mainly of zero-valent oxidation state and no significant oxidation took place under atmospheric conditions for weeks. Characterization with HR-TEM showed that each iron nanoparticle is consisted of a core that contains iron in its zero-oxidation state, and an iron oxide shell surrounding it that is <3 nm thick. Iron nanoparticles demonstrated chain like morphologies due to their strong magnetic interactions.

nZVI was applied as a sorbent for aqueous Ni^{2+} and Cd^{2+} ions under different conditions. According to results, nZVI demonstrated fast uptake kinetics and outstanding uptake capacities. On the overall, Ni^{2+} ions were adsorbed in larger quantities compared to Cd^{2+} ions. Repetitive applicatios showed that nZVI can be used for sucessive trials for the removal of Cd^{2+} ions at low concentrations. However, the same was not observed for Ni^{2+} ions the uptake of which caused deterioration of the adsorption capacity of the material after the first trial. The extent of uptake of both ions was not seriously affected by pH variations in the pH range 4.0 to 10.0.

The uptake of these ions was compared with that of Cu^{2+}, Zn^{2+}, and Sr^{2+} ions to test the effect of the reduction potential and/or charge density on the extent of uptake. Acoording to results for concentration range between 10.0 mg/L to 100.0 mg/L the priority of fixation by nZVI for the studied cations followed the order: $Cu^{2+}>Ni^{2+}>Cd^{2+}>Zn^{2+}>Sr^{2+}$. Never the less, the same sequence was not verified at higher initial concentrations of the cations, and the charge density of the cations appeared to be increasingly effective in determining the extent of the uptake.

The XPS surveys showed that both of Ni^{2+} and Cd^{2+} ions did not undergo oxidation-reduction mechanism upon exposure to nZVI. Both of the ions are most probably fixed by a complexation mechanism to the oxygen atoms in the oxohydroxyl groups at the shell surface of the nanoparticles.

The desorption behavior was also studied in order to assess the stability of uptake. While the transition metals demonstrated stable adsorption in particular at lower

concentrations (up to 100.0 mg/L), the uptake of Sr^{2+} uptake was highly unstable at all concentrations, the thing that was referred to a different adsorption mechanism in which weak electrostatic forces seems to be operative (physical adsorption).

On the overall, the performed studies indicate that zero-valent iron nano particles are very effective in the removal of the studied cations. More work is still, however, required to get better understanding of the uptake mechanisms, in particular for cations that possess standard electrode potentials close to the energy of the conduction band of the iron oxide.

REFERENCES

Alloway, B.J. 1995. *Heavy Metals in Soils-Second Edition.* Blackie Academic and Professional

Baird, Colin. 2001. *Environmental Chemistry - Second Edition*. W.H. Freeman and Company.

Balko, B.A., Tratnyek, P.G. 1998. Photoeffects on the reduction of carbon tetrachloride by zero-valent iron. *J. Phys. Chem. B* 102:1459-1465.

Blowes, D.W., Ptacek, C.J., Benner, Shawn G., McRae, Che W.T, Bennett, T.A., Puls, R.W. 2000. Treatment of inorganic contaminants using permeable reactive barriers. *Journal of Contaminant Hydrology* 45:123-137.

Chemistry : Periodic Table : iron : standard reduction potentials. 2008. Web of Elements. http://www.webelements.com/webelements/elements/text/Fe/redn.html (accessed Septemer 30, 2007)

Cook, M. E.,Morrow, H., 1995 "*Anthropogenic Sources of Cadmium in Canada," National Workshop on Cadmium Transport Into Plants*, Canadian Network of Toxicology Centres, Ottawa, Ontario, Canada, .

Üzüm Ç., Shahwan T., Eroğlu A. E., Lieberwirth I., Scott T. B., Hallam K. R., 2008. Application of zero-valent iron nanoparticles for the removal of aqueous Co^{2+} ions under various experimental conditions, Accepted for publication by *Chem. Eng. J.*, In press.

Karabelli D., Uzum Ç., Shahwan T., Eroğlu A. E., Scott T., Hallam K., Lieberwirth I, 2008. Batch Removal of Aqueous Cu^{2+} Ions Using Nanoparticles of Zero-Valent Iron: A Study of the Capacity and Mechanism of Uptake, *Ind. & Eng. Chem. Res.*, In press.

Electron Energy Loss Spectroscopy. 2008. Kyoto University. http://eels.kuicr.kyoto-u.ac.jp/eels.en.html (accessed May 10, 2008).

Evangelou, V.P. 1998. *Environmental Water and Soil Chemistry - Principles and Applications*. New York: John Wiley & Sonc, Inc.

Feynmans Classic Talk. 2008. Renssealer Polytechnic Institute. http://www.rpi.edu/dept/materials/COURSES/NANO/shaw/Page5.html (accessed May 30, 2008).

Kanel, S.R., Greneche, J., Choi, H. 2006. Arsenic(V) Removal from Groundwater Using Nano Scale Zero-Valent Iron as a Colloidal Reactive Barrier Material. *Environmental Science & Technology* 40:2045-2050.

Kanel, S.R., Manning, B., Charlet, L., Choi, H. 2005. Removal of Arsenic(III) from Groundwater by Nanoscale Zero-Valent Iron. *Environmental Science & Technology* 39:1291-1298.

Kim K.S., Winograd N.1974. X-ray photoelectron spectroscopic studies of nickel-oxygen surfaces using oxygen and argon ion-bombardment *Surface Science.* 43:625-643.

Kishi K.1998. Adsorption of ethylenediamine on clean and oxygen covered Fe/Ni(100) surfaces studied by XPS *Journal of Electron Spectroscopy and Related Phenomena* 46:237-247.

Kishi K., Fujita T. 1990. Interaction of Ni/Cu(100) surfaces with O_2 studied by XPS *Surface Science* 227:107-113.

Kishi K., Ikeda S.1973. X-Ray Photoelectron Spectroscopic Study for the Reaction of Evaporated Iron with O_2 and H_2O *Bulletin of the Chemical Society of Japan* 46:341-345.

Korea Atomic Energy Research Institute. 2008. http://www.kntc.re.kr/Cyberserver/openlec/nuke(2)/nuclearfeul/nuclearfeul_13/ch13_4.html (accessed April 11, 2008).

Li C.P., Proctor A., Hercules D.M. 1984. Curve Fitting Analysis of ESCA Ni 2p Spectra of Nickel-Oxygen Compounds and Ni/Al_2O_3 Catalysts.*Applied Spectroscopy*. 38:880–886.

Li, L., Fan, M., Brown, R.C., van Leeuwen, L. 2006. Synthesis, Properties, and Environmental Applications of Nanoscale Iron-Based Materials: A Review. *Critical Reviews in Environmental Science and Technology* 36:405-431.

Li, X., Brown, D.G., Zhang, W. 2007. Stabilization of biosolids with nanoscale zerovalent iron (nZVI). *Journal of Nanoparticle Research* 9:233-243.

Li, X. and Zhang, W. 2006. Iron Nanoparticles: the Core-Shell Structure and Unique Properties for Ni(II) Sequestration. *Langmuir* 22:4638-4642.

Li, X. and Zhang, W. 2007. Sequestration of Metal Cations with Zerovalent Iron Nanoparticless: A Study with High Resolution X-ray Photoelectron Spectroscopy (HR-XPS). *Journal of Physical Chemistry C* 111(19):6939-6946.

Lorenz P., Finster J., Wendt G., Salyn J.V., Zumadilov E.K., Nefedov V.I.1979. J. *Electron Spectrosc. Relat. Phenom*. 16:267-276.

Loechel B.P., Strehblow H.H.1984. Breakdown of Passivity of Nickel by Fluoride. *J. Electrochem. Soc*. 131:713-723.

Manahan, S.E. 1991. *Environmental Chemistry, 5th ed*. Chelsea, MI: Lewis Publishers.

McIntyre, N.S. and Cook, M.G. 1975. X-ray photoelectron studies on some oxides and hydroxides of cobalt, nickel, and copper. *Analytical Chemistry* 47:2208-2213.

N.S. McIntyre and M.G. Cook.1975. X-ray photoelectron studies on some oxides and hydroxides of cobalt, nickel, and copper, *Anal. Chem.* 47:2208-2213.

Nurmi, J.T., Tratnyek, P.G., Sarathy, G., Baer, D.R., Amonette, J.E., Pecher, K., Wang, C., Linehan, J.C., Matson, M.W., Penn, R.L., Driessen, M.D. 2005. Characterization and Properties of Metallic Iron Nanoparticles: Spectroscopy, Electrochemistry, and Kinetics. *Environmental Science & Technology* 39:1221, 1230.

Salvati L., Makovsky L.E., Stencel J.M., Brown F.R., Hercules D.M.1998. Surface Spectroscopic Study of Tungsten-Alumina Catalysts Using X-ray Photoelectron, Ion Scattering, and Raman Spectroscopies *J. Phys. Chem*. 85:3700-3707.

Skoog, D.A., Holler, F.J., Nieman, T.A. 1998. *Principles of Instrumental Analysis*. USA: Brooks/Cole Thomson Learning.

S.M. Ponder, J.G. Darab and T.E. Mallouk 2000. Remediation of Cr(VI) and Pb(II) aqueous solutions using nanoscale zero-valent iron, *Environ. Sci. Technol.* 34:2564-2569.

S.R Kanel, B. Manning, L. Charlet and H. Choi. 2005. Removal of arsenic(III) from groundwater by nanoscale zero-valent iron, *Environ. Sci. Technol.* 39:1291-1298.

S.R. Kanel, J.M. Greneche and H. Choi. 2006. Arsenic(V) removal from groundwater using nano scale zero-valent iron as a colloidal reactive barrier material, *Environ. Sci. Technol.* 40:2045-2050.

Sun, Y., Li, X., Cao, J., Zhang, W., Wang, H.P. 2006. Characterization of zero-valent iron nanoparticles. *Advances in Colloid and Interface Science* 120:47-56.

Ponder, S.M., Darab, J.G., Mallouk, T.E. 2000. Remediation of Cr(VI) and Pb(II) Aqueous Solutions Using Supported, Nanoscale Zero-valent Iron. *Environmental Science & Technology* 34:2564–2569.

Thiruvenkatachari, R., Vigneswaran, S., Naidu, R. 2007 Permeable reactive barrier for groundwater remediation. *Journal of Industrial and Engineering Chemistry* 14:145–156

The Transmission Electron Microscope. 2008. Nobel Web AB. http://nobelprize.org/educational_games/physics/microscopes/tem/index.html (accessed May 10, 2007).

Tratnyek, P.G and Johnson, R.L. 2006. Nanotechnologies for environmental cleanup. *Nano Today* 1(2):44-48.

U.S. Department of the Interior, U.S. Geological Survey. 2001. USGS OFR01-041: Xray Diffraction Primer. http://pubs.usgs.gov/of/2001/of01-041/htmldocs/xrpd.htm (accessed May 30, 2008).

Wagner, C.D., Riggs, W.M., Davis, L.E., Moulder, J.F., Muilenberg, G.E. 1979. *Handbook of X-Ray Photoelectron Spectroscopy, Perkin-Elmer Corporation, Physical Electronics Division*. Minn. 55344: Eden Prairie.

Wang, C. and Zhang, W. 1997. Synthesizing Nanoscale Iron Particles for Rapid and Complete Dechlorination of TCE and PCBs. *Environmental Science & Technology* 31(7):2154-2156.

Wang, W., Jin, Z., Li, T., Zhang, H., Gao, S. 2006. Preparation of spherical iron nanoclusters in ethanol–water solution for nitrate removal. *Chemosphere* 65:1396-1404.

Wang, X., Wang, J., Sun, C 2006. Removal of Copper(II) Ions from Aqueous Solutions Using Natural Kaolinite. *Adsorption Science & Technology* 24(6):517:530.

Wikipedia contributors, "Nickel". 2008a. Wikipedia, The Free Encyclopedia. http://en.wikipedia.org/wiki/Nickel (accessed May 29, 2008).

Wikipedia contributors, "Copper". 2008b. Wikipedia, The Free Encyclopedia. http://en.wikipedia.org/wiki/Copper (accessed May 29, 2008).

Wikipedia contributors, "Copper". 2008c. Wikipedia, The Free Encyclopedia. http://en.wikipedia.org/wiki/Copper (accessed May 29, 2008).

Wikipedia contributors, "Stronsium". 2008d. Wikipedia, The Free Encyclopedia. http://en.wikipedia.org/wiki/Stronsium (accessed May 29, 2008).

Wikipedia contributors, "Zinc". 2008e. Wikipedia, The Free Encyclopedia. http://en.wikipedia.org/wiki/Zinc (accessed May 29, 2008).

Wikipedia contributors, "Iron". 2008f. Wikipedia, The Free Encyclopedia. http://en.wikipedia.org/wiki/Iron (accessed May 30, 2008).

Wikipedia contributors, "Transmission Electron Microscopy". 2008g. Wikipedia, The Free Encyclopedia. http://en.wikipedia.org/wiki/Transmission_electron_microscopy (accessed May 10, 2008).

X.Q. Li and W.X. Zhang. 2006. Iron nanoparticles:The core-shell structure and unique properties for Ni(II) sequestration. *Langmuir* 22:4638-4642.

X.-Q. Li and W.X. Zhang 2007. Sequestration of metal cations with zerovalent iron nanoparticles - A study with high resolution x-ray photoelectron spectroscopy (HR-XPS), *J. Phys. Chem. C.* 111:6939-6946.

Zhang, W. 2003. Nanoscale iron particles for environmental remediation: An overview. *Journal of Nanoparticle Research* 5:323-332.

Zhang W and Elliot, D.W. 2006. Applications of Iron Nanoparticles for Groundwater Remediation. *REMEDIATION* Spring 2006:7-21.

Zhang, H., Jin, Z., Han, L., Qin, C. 2006. Synthesis of nanoscale zero-valent iron supported on exfoliated graphite for removal of nitrate. *Transactions of Nonferrous Metals Society of China* 16:345-349.